이학박사 학위논문

# The Role of Upper-Troposphere and Stratosphere Ozone in the Tropical Temperature Bias and Extratropical Predictability in the Operational Models

적도 기온 편차와 중위도 예측성에 미치는
상부대류권과 성층권 오존의 역할

2022년 8월

서울대학교 대학원
지구환경과학부

오지영

# The Role of Upper-Troposphere and Stratosphere Ozone in the Tropical Temperature Bias and Extratropical Predictability in the Operational Models

**By**
**Jiyoung Oh**

**A Dissertation submitted to the Faculty of the Graduate School of the Seoul National University in partial fulfillment of the requirements for the Degree of Doctor of Philosophy**

**Degree Awarded:**
**June 2022**

**Advisory committee:**

**Professor Wookap Choi, Chair**
**Professor Seok-Woo Son, Advisor**
**Professor Rokjin Park**
**Doctor Yoonjae Kim**
**Professor Joowan Kim**

# The Role of Upper-Troposphere and Stratosphere Ozone in the Tropical Temperature Bias and Extratropical Predictability in the Operational Models

## 적도 기온 편차와 중위도 예측성에 미치는 상부대류권과 성층권 오존의 역할

지도교수 손석우

이 논문을 이학박사 학위논문으로 제출함

2022년 6월

서울대학교 대학원
지구환경과학부
오지영

오지영의 이학박사 학위논문을 인준함
2022년 6월

위원장 _____(인)
부위원장 _____(인)
위 원 _____(인)
위 원 _____(인)
위 원 _____(인)

# Abstract

Oh, Jiyoung
School of Earth Environmental Sciences
The Graduate School
Seoul National University

A systematic warm bias in the tropical tropopause layer (TTL) is commonly found in both climate and numerical weather prediction models. In this study, the nature of this temperature bias is examined by integrating the MetOffice Unified Model (MetUM) with various ozone concentrations in the TTL. Like other models, the long-term integration of MetUM with the Atmospheric Model Intercomparison Project (AMIP) configuration shows a notable warm bias (~2 K) in the TTL with a comparable cold bias in the tropical stratosphere above ~70 hPa. We demonstrate that these biases are particularly sensitive to the tropical ozone concentration prescribed in the model. By replacing the background ozone, which is typically used for AMIP-type simulations, with the Southern Hemisphere ADditional OZonesondes (SHADOZ) measurements or the Binary Data Base of Profiles (BDBP), the dipolar temperature biases in the TTL and tropical stratosphere are significantly reduced. Further sensitivity tests show that the tropical ozone amount in a 14–20 km layer is a key contributor to this change. These results suggest that accurate ozone forcing in

the TTL is crucial for reliable weather and climate simulations.

Recent studies have shown that Madden-Julian Oscillation (MJO) is modulated by Quasi-Biennial Oscillation (QBO) during the boreal winter; MJO becomes more active and predictable during the easterly phase of QBO (EQBO) than the westerly phase (WQBO). Despite growing evidences, climate models fail to capture the QBO-MJO connection. One of the possible reasons is a weak static stability change in the upper troposphere and lower stratosphere (UTLS) by neglecting QBO-induced ozone change in the model. Here, we investigate the possible impact of the ozone–radiative feedback in the tropical UTLS on the QBO-MJO connection by integrating the Global Seasonal Forecasting System 5 (GloSea5) model. A set of experiments are conducted by prescribing either the climatological ozone or the observed ozone at a given year for the EQBO-MJO event in January 2006. The realistic ozone improves the temperature simulation in the UTLS. However, its impacts on the MJO are not evident. The MJO phase and amplitude do not change much when the ozone is prescribed with observation. While it may suggest that the ozone-radiative feedback plays a rather minor role in the QBO-MJO connection, it could also result from model biases in UTLS temperature and not-well organized MJO in the model.

Antarctic ozone has been regarded as a major driver of the Southern Hemisphere (SH) circulation change in the recent past. Here, we show that Antarctic

ozone can also affect the subseasonal-to-seasonal (S2S) prediction during the SH spring. Its impact is quantified by conducting two reforecast experiments with GloSea5. Both reforecasts are initialized on September 1st of each year from 2004 to 2020 but with different stratospheric ozone: one with climatological ozone and the other with year-to-year varying ozone. The reforecast with climatological ozone, which is common in the operational S2S prediction, shows the skill re-emergence in October after a couple of weeks of no prediction skill in the troposphere. This skill re-emergence, mostly due to the stratosphere-troposphere dynamical coupling, becomes stronger in the reforecast with year-to-year varying ozone. The surface prediction skill also increases over Australia. This result suggests that a more realistic stratospheric ozone could lead to improved S2S prediction in the SH spring.

**Keywords:** Stratosphere-troposphere coupling, ozone-radiative feedback, QBO-MJO, Subseasonal-to-seasonal prediction, temperature bias

**Student Number:** 2009-30863

# Table of Contents

# List of Tables

# List of Figures

Dark, dashed and light curves indicate CTR, BDBP and SOZ, respectively.

**Figure 1.5**. Longitude-pressure distributions of temperature difference between CTR and other ozone experiments: (a) SOZ, (b) BDBP, (c) SOZ_TTL, and (d) BDBP_TTL. Shading and contour interval are 0.2 K and 0.5 K.

**Figure 2.1.** Time-pressure cross section of (a) monthly zonal-mean zonal wind (m $s^{-1}$), (b) temperature anomalies (K) and (c) ozone (ppmv) averaged over 10°S–10°N.

**Figure 2.2.** Latitude-pressure distribution of (a) zonal wind anomalies (m $s^{-1}$), (b) temperature (K) and (c) zonal-mean ozone (%) in EQBO winter of January–February 2006.

**Figure 2.3.** Differences in zonal-mean zonal wind (m $s^{-1}$) and temperature (K) (a), (d) between COZ and observed climatology, (b), (e) between YOZ and observed climatology, and (c), (f) between YOZ and COZ experiments averaged over January–February 2006.

**Figure 2.4.** Longitude-time sections of zonal-mean temperature (K) averaged from 15°S to 5°N in (a) observation, (b) COZ, (c) YOZ, and (d) their difference in Janurary–February 2006.

**Figure 2.5.** Longitude-time sections of bandpass-filtered (20–100 days) OLR (W m-1) averaged from 15°S to 5°N in (a) observation, (b) COZ, (c) YOZ and (d) the difference between YOZ and COZ. Temporal evolution is shown from 1 January to 6 February, 2006 when MJO is well defined in observation.

statistically significant at the 95% confidence level. (c), (d) Same as (a), (b) but for PCI predicted by a linear regression model based on 10-hPa PCI on 1st September.

**Figure 3.5.** Anomaly correlation coefficients (ACCs) of 14-day running averaged PCI as a function of forecast lead time in (a) COZ and (b) YOZ experiments for the period of 2004–2020. The values which are statistically significant at the 95% confidence level are dotted. (c) ACCs of 700-hPa PCI in COZ experiment in black and those in YOZ experiment in red. Open circles denote the values which are statistically significant at the 95% confidence level. The forecast time when the ACC difference (YOZ minus COZ) is statistically significant at the 95% confidence level is shaded in pink. Note that October 6 in x-axis refers to the ACC at the forecast week 6–7.

**Figure 3.6.** Same as of Fig. 3.4a but for four models archived for the S2S prediction. (a) Bureau of Meteorology, (b) China Meteorological Administration (CMA), (c) Centre National de Recherches Météorologiques (CNRM) of Météo-France, (d) European Centre for Medium-Range Weather Forecasts (ECMWF) and (e) United Kingdom Met Office (UKMO). The reforecast period is denoted at the top of each panel.

**Figure 3.7.** (a) Root-mean-squared error (RMSE) (m) and (b) ACC of 700-hPa PCI at the forecast week 6–7 in COZ and YOZ experiments. (c), (d) ACCs of week 6–7 PCI700 as a function of ensemble size and number of validation years. Each line indicates the average value of bootstrap-generated 1,000 ACCs. Square indicates the practical ACC shown in (b). Bars represent p-values for the ACC difference (YOZ minus COZ). The

# Overview

The upper-troposphere and lower stratosphere (UTLS) is a transition layer between troposphere and stratosphere, which exhibits the local minimum temperature and irregular mixings of many chemical components such as ozone and water vapour. However, most operational models use ozone climatology. It induces the temperature biases in the tropics and polar region and affects the global radiation budget (e.g. Fueglistaler et al. 2009; Gettelman et al. 2004).

In order to evaluate the impact of UTLS ozone, it is investigated in terms of temperature biases and the predictability. In Chapter 1, temperature bias in the tropical tropopause layer is examined by integrating atmosphere-only model with various ozone concentration. Chapter 2 and 3 focus on the impact of UTLS ozone on the stratosphere-troposphere coupling in tropics and Southern Hemisphere. The contents in Chapter 1 and 3 are published in Oh et al. (2018) and Oh et al. (2022), respectively. Chapter 2 is based on Oh et al. (2022), which is under review.

# 1. Ozone sensitivity of tropical upper-troposphere and stratosphere temperature

## 1.1. Introduction

The tropical tropopause layer (TTL), typically defined as being from ~14 km to ~18.5 (~150–70 hPa), is characterized by a sharp change in thermal structure and chemical composition (Fueglistaler et al. 2009). Properties of the TTL are influenced by both tropospheric and stratospheric processes (Fueglistaler et al. 2009; Lin et al. 2016), as the TTL is a transition zone between the tropospheric and stratospheric zones. The unique thermal structure of the TTL is primarily determined by large-scale dynamical and radiative processes, among others. In general, dynamical cooling induced by the lower-stratospheric upward branch of the Brewer-Dobson circulation (Brewer, 1949; Dobson, 1956) is known to drive the cold point in the TTL. This dynamical cooling is largely offset by radiative heating (e.g., Fueglistaler et al. 2009; Kim and Son, 2015). This balance between the two processes is an important factor in understanding temperature variability in the TTL, and has motivated many relevant studies (e.g., Randel and Jensen, 2013).

Although significant progress has been made in modelling the TTL, many climate models and numerical weather prediction models still suffer from significant temperature biases in the TTL (e.g., Hardiman et al. 2015). Cordero and Forster

(2006) and Kim et al. (2013) reported that the coupled climate models that have been used in the Coupled Model Intercomparison Project (CMIP) Phase 3 or 5 have larger temperature biases in the TTL than in the mid-troposphere. In particular, most models show cold biases in the mid-troposphere but warm biases around the tropopause (～2 K at 100 hPa in terms of the multi-model mean). These biases are not peculiar to just coupled climate models. A similar bias is also found in operational numerical weather prediction models. By integrating the MetOffice Unified Model (MetUM) with the Atmospheric Model Intercomparison Project (AMIP) configuration, Hardiman et al. (2015) found the same temperature bias in the TTL as in Phase 5 of the Coupled Model Intercomparison Project (CMIP5) models.

The warm biases in the TTL could be caused by multiple factors. As one possibility, the present study explores the possible role of ozone bias in the TTL. It is well documented that ozone (along with water vapour and carbon dioxide) is the key factor that controls the radiative budget in the TTL and tropical stratosphere (e.g., Thuburn and Craig, 2002; Gettelman et al. 2004). Both observational and modelling studies have shown a close relationship between the ozone and TTL temperatures. Chae and Sherwood (2007), in their one-dimensional radiative-convective model simulations, reported that ozone is the key factor that determines the seasonal cycle of TTL temperatures. Fueglistaler et al. (2011) further demonstrated that interactive ozone is crucial in reproducing the annual cycle and interannual variability of TTL

temperatures. In particular, they pointed out that dynamically induced ozone variation and its feedback are important for understanding the seasonal cycle of TTL temperatures. More recently, Ming et al. (2017) reported that over 30% of the seasonal cycle of TTL temperatures is controlled by the radiative effect of seasonally varying ozone in the TTL. All of these results suggest that accurate ozone radiative forcing is crucial for modelling realistic TTL temperatures.

In this study, the importance of ozone in the TTL temperature bias is evaluated by integrating the MetUM with various tropical ozone concentrations. This model has higher horizontal and vertical resolutions and more comprehensive physics than conventional climate models, and allows us to better understand the physical processes responsible for temperature biases in the TTL. By systematically varying tropical ozone concentration in the model, it is shown that an excessively high ozone concentration in the TTL causes significant warm biases in the TTL and cold biases in the tropical stratosphere.

## 1.2. Data and methods

### 1. 2. 1. Observational data: SHADOZ and BDBP

Many satellites ozone-measurement have been releasing their products since 1970. However, ground-based network data such as ozonesonde as a reference are used to verify their profiles and total column ozone measurements (Davis et al. 2016). Also, it is very useful in the UTLS region, especially in the tropics. Ozonesonde observations performed at various points on the equator, such as Southern Hemisphere ADditional OZonesondes (SHADOZ, Thompson et al. 2003), have provided an opportunity to better understand the vertical structure of ozone and its associated large-scale circulation.

In Chapter 1, SHADOZ data is implied on the climatological ozone ancillary for the sensitivity simulations. SHADOZ project was launched since 1998 (http://tropo.gsfc.nasa.gov/shadoz) with an international collaboration and has been collecting a number of ozonesonde data in the tropics and subtropics. Therefore, SHADOZ data are very helpful to understand the tropical features. Also, it is continuously used to evaluate the satellite-retrieval data and the data assimilation for chemical transport models (more detail information in Davis et al. 2016).

The zonal-mean monthly mean SHADOZ ozone is constructed from 13 tropical stations (table 1.1) located within 30°S–30°N (a full list of the stations can be found in Thompson et al. 2003, table 2).

The gridded ozone data is also tested using the Binary Data Base of Profile (BDBP; Bodeker et al. 2013, http://bodekerscientific.com). The BDBP is a merged ozone product from ozonesondes and multiple satellite measurements including the SAGE-I and II, HALOE, the Limb Infrared Monitor of the Stratosphere (LIMS) and the Improved Limb Array Spectrometer (ILAS)-I and II (Hassler et al. 2008; Bodeker et al. 2013). The tier-0 BDBP ozone is used for the experiment and has a 5° resolution in latitude and 70 vertical layers from 1 to 70 km (1-km vertical spacing, 878.4 hPa to 0.046 hPa). The current BDBP data is available for the period 1979–2016 and the Tier 1.4 monthly mean data for the period of 1979–2007 are used in Chapter 1.

**Table 1.1.** SHADOZ observation sites.

| Observation Station | Latitude/Longitude | | Periods |
|---|---|---|---|
| Ascension Is. | 8.0°S | 14.4°W | 1998–2008 |
| Costa Rica (various sites) | 10.0°N | 84.0°W | 2005–2008 |
| Hanoi of Vietnam | 21.02N | 105.8°E | 2004–2008 |
| Hilo of Hawaii | 19.4°N | 155.4°W | 1998–2008 |
| Irene of South Africa | 25.9°S | 28.2°E | 1998–2008 |
| La Reunion Is. of France | 21.1°S | 55.5°E | 1998–2008 |
| Kuala Lumpur of Malaysis | 2.7°N | 101.7°E | 1998–2008 |
| Nairobi of Kenya | 1.3°S | 36.8°E | 1998–2008 |
| Natal of Brazil | 5.4°S | 35.4°W | 1998–2008 |
| Paramaribo of Surinam | 5.8°N | 55.2°W | 1999–2008 |
| Pago Pago of Samoa | 14.4°S | 170.6°W | 1998–2008 |
| San Cristobal of Ecuador | 0.9°S | 89.6°W | 1998–2008 |
| Suva of Fiji | 18.1°S | 178.4°E | 1998–2008 |

## 1. 2. 2. SPARC ozone data

The SPARC ozone dataset is produced by merging satellite-based observational data in the stratosphere with model-based ozone estimations in the troposphere. More specifically, the stratospheric ozone is determined by combining multiple satellite observations and polar ozonesonde measurements (Randel and Wu, 2007) with the seasonally varying ozone climatology from Fortuin and Kelder (1998). In contrast, tropospheric ozone is estimated by averaging ozone products modelled from the Community Atmospheric Model version 3.5 (CAM3.5; Lamarque et al. 2010) and the NASA Goddard Institute for Space Studies model for Physical Understanding of Composition-Climate Interaction and Impacts (GISS-PUCCINI; Shindell et al. 2006). Since tropospheric ozone has a large difference in its spatial and temporal distribution locally, it is not appropriate to apply the same linear regression method with the satellite observations. These two different estimations are then merged near the tropopause using a log-linear interpolation. Further details are provided in Cionni et al. (2011).

For the control simulations in chapter 1, ozone data is taken from the zonal-mean time-varying ozone dataset of the Atmospheric Chemistry and Climate/Stratospheric Processes and their Role in Climate (AC&C/SPARC, Cionni et al. 2011). This dataset, referred to as SPARC ozone, has been widely used in AMIP and CMIP5 simulations. UKMO uses the climatological AC&C/SPARC ozone data

in their operational models, including numerical and subseasonal-to-seasonal scale model, for the period of 1994–2005, which is matched with the 12-year period of the UKMO operational stratospheric analysis record (Bushell et al. 2010).

## 1.2.3. Model description

The numerical model used in this study is the Global Atmosphere 7.0 (GA7) configuration of the MetUM. The horizontal resolution is ～1.875° longitude and ～1.25° latitude. In the vertical resolution, 85 model levels are employed, 50 of which are in the troposphere and 14 of which are in the upper troposphere and lower stratosphere (UTLS, ～11–20 km). The aver- age level spacing in the TTL is about 665 m. As in Hardiman et al. (2015), this model is integrated into the AMIP configuration by prescribing chemistry and surface boundary conditions. Daily sea surface temperatures, sea ice distributions and monthly climatology land surface conditions are used in all model experiments (Reynolds et al. 2007). State-of-the-art physical parameterizations are adopted in this model. The radiation scheme, among others, is taken from Edwards and Slingo (1996) with several modifications (Cusack et al. 1999). This scheme uses six bands for shortwave with ozone, water vapour, carbon dioxide and oxygen, and nine bands for longwave with methane, nitrous oxide and chloro- and hydrofluorocarbon species, along with ozone, water vapour and carbon dioxide. While water vapour is prognostic in the model, ozone is simply prescribed. Other species are either fixed or time-varying as described in Hardiman et al. (2015).

## 1.2.4. Experimental design

Considering that the SPARC ozone in the TTL is largely a model product, a series of experiments are conducted in which the SPARC ozone is replaced with long-term ozonesonde observations. The control run (CTR) utilizes the default ozone data from the SPARC database. In the sensitivity run (SOZ) with the Southern Hemisphere ADditional OZonesondes (SHADOZ; Thompson et al. 2003) data, tropical ozone concentrations from surface to 20 km within 30°S–30°N are replaced by the ozonesonde observations from the SHADOZ data. The zonal-mean monthly mean SHADOZ ozone is constructed from 13 tropical stations located within 30◦S–30◦N (a full list of the stations can be found in Thompson et al. 2003, table 2). In order to identify the role of the TTL ozone, the experiment is repeated with SHADOZ ozone but only over a depth of 14–20 km (referred to as SOZ_TTL).

Using BDBP data, additional sensitivity tests to tropical ozone (30°S–30°N) are conducted. In these runs, the tropical ozone is replaced with the BDBP data (referred to as BDBP and BDBP_TTL) instead of the SHADOZ ozone data.

All of these experiments, i.e., CTR, SOZ, SOZ_TTL, BDBP and BDBP_TTL, are integrated for a 20-year period from 1989 to 2008 with climatological surface boundary conditions. Apart from the ozone data, all the configurations are identical in these simulations.

Temperature and humidity biases are evaluated from the European Centre for Medium-Range Weather Forecasts (ECMWF) Interim Reanalysis (ERAI; Dee et al. 2011) and the NASA Modern-Era Retrospective Analysis for Research and Applications version 2 (MERRA-2; Bosilovich et al. 2015). The Stratospheric Water and Ozone Satellite Homogenized (SWOOSH) dataset (Tummon et al. 2015; Davis et al. 2016) is also used to supplement the ozone and stratospheric water vapour evaluation. For these evaluations, the 20-year period from 1989 to 2008 is used to match the model integration period.

### 1.2.5. Tendency analysis tool

The temperature budget analysis is based on the thermodynamic energy equation. It is written as below (Equation from Fueglistalier et al. 2009b):

$$\frac{\partial T}{\partial t} = -V_H \cdot \nabla_H T + \omega\left(\frac{\kappa T}{p} - \frac{\partial T}{\partial p}\right) + \frac{Q}{c_p}$$

$$\frac{Q}{c_p} = \frac{Q_{rad}}{c_p} + \frac{Q_{res}}{c_p}$$

where $\partial T/\partial t$ is the temperature tendency, $-V_H \cdot \nabla_H T$ is the horizontal advection of temperature, $\omega(\kappa T/p - \partial T/\partial p)$ is the vertical advection of temperature, and $Q/C_p$ is the diabatic heating and cooling term. The last heating and cooling term can be divided the radiative heating term and the residual term consisted of latent heating exchange with diffusive and turbulent heat transport including numerical errors.

## 1.3. Results

### 1.3.1. Temperature biases in the tropical tropopause

Figure 1.1a presents the latitude-pressure distribution of the temperature bias in the CTR run. This experiment shows strong temperature biases in the upper troposphere and stratosphere compared to the reanalyses (only the evaluation against ERAI is presented here because the model biases against MERRA-2 essentially show the same results). In the tropics, warm biases from ~200 to ~70 hPa and cold biases above ~70 hPa are evident. In the extratropics, distinct cold biases appear in the lower stratosphere in both hemispheres. Strong temperature biases are also present in the extratropical mid- to upper stratosphere. These biases appear persistently in the course of the model simulations. Although the extratropical temperature biases are an important issue as they also appear in the coupled climate models (e.g., fig. 4 of Reichler and Kim, 2008; fig. 2 of Charlton-Perez et al. 2013), we focus on the tropical region in this study. The extratropical bias will be analyzed in a future study.

In the TTL, warm biases are consistently found during the entire period of integration, with a maximum value of up to ~2 K. As discussed earlier, similar temperature biases have been reported in the climate models used in the CMIP3 (Cordero and Forster, 2006) and CMIP5 (Kim et al. 2013). They are also observed

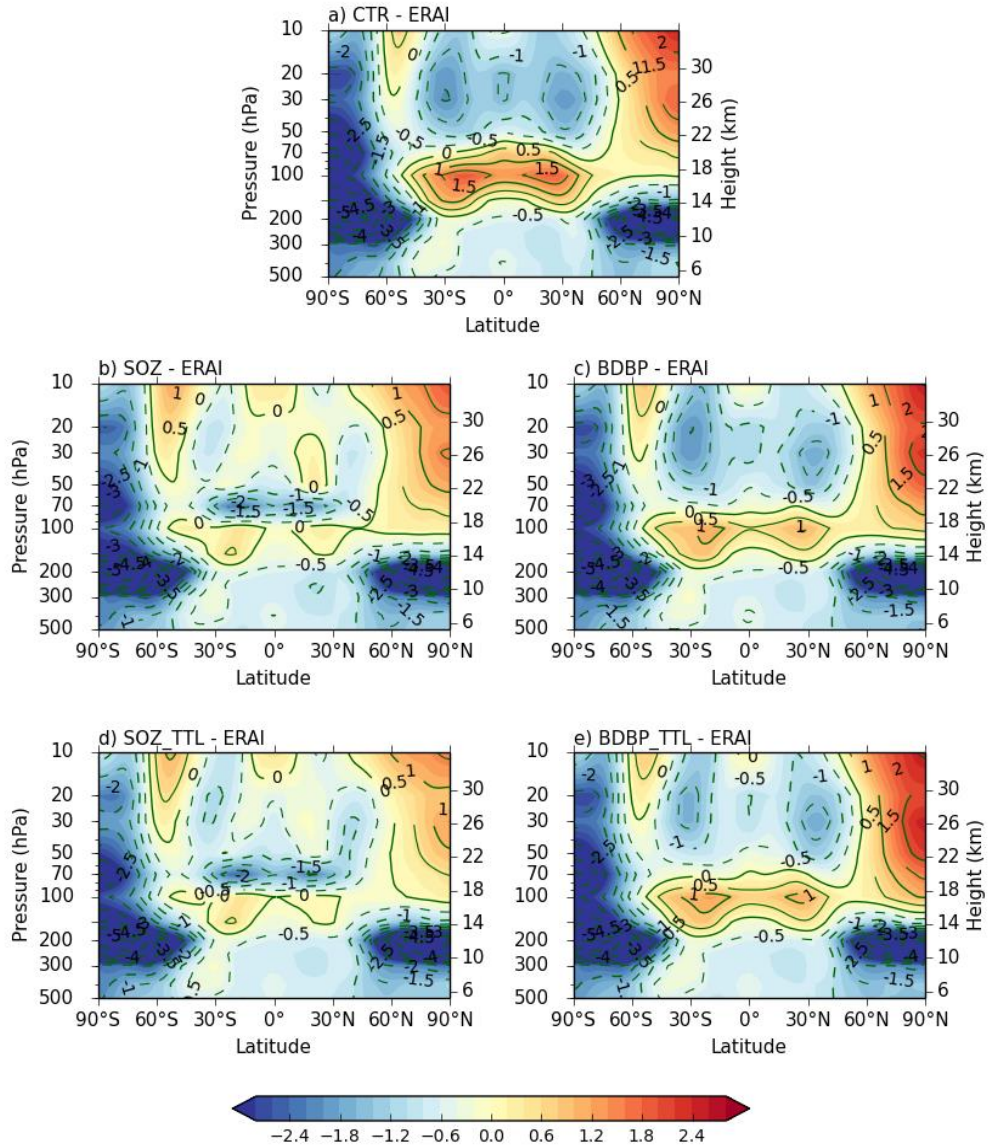


**Figure 1.1.** Latitude-pressure distributions of zonal-mean temperature bias for the 20-year (1989-2008) AMIP simulations: (a) CTR, (b) SOZ, (c) BDBP, (d) SOZ_TTL and (e) BDBP_TTL. The biases are computed from ERAI temperature for the same period. Shading and contour intervals are 0.2 K and 0.5 K, respectively.

in various versions of the MetUM (Hardiman et al. 2015). Although the cause(s) of the warm biases could vary among the models, similar temperature biases in many different models imply that warm biases may have similar causes (Hardiman et al. 2015). In these simulations, warm biases could be caused by an unrealistic ozone concentration in the TTL. By analysing the chemistry-climate models archived for the Chemistry-Climate Model Validation Phase 2 (CCMVal2) project, Birner and Charlesworth (2017) reported that the temperature in the tropical tropopause is strongly correlated with the amount of ozone in the TTL. Hardiman et al. (2015) further showed that the TTL temperature in the MetUM simulation with interactive chemistry has strong sensitivity to ozone concentration in the TTL. They reported that the overestimated TTL ozone (up to 80%) in their interactive chemistry run could cause additional warm biases of up to ~2.5 K in the TTL.

The influence of the ozone difference on the TTL temperature is tested by integrating the MetUM with different ozone data. The SPARC ozone is simply replaced with monthly mean SHADOZ and BDBP ozone in the tropical troposphere and lower stratosphere from the surface to ~20 km from 30°S to 30°N (SOZ and BDBP runs). Except in this region, the SPARC ozone is prescribed as in the CTR run. With this modification, the AMIP-type experiments are conducted for the 20-year period.

The temperature biases in the SOZ run are illustrated in Figure 1.1b. The warm biases in the TTL largely disappear. Only relatively small warm biases of ~0.5 K are found in the subtropical upper troposphere. The broad cold biases in the tropical lower stratosphere are also reduced significantly, indicating that not only TTL warm biases but also tropical stratospheric cold biases are partly related to an ozone concentration below ~20 km.

### 1.3.2. Comparison between observations and SPARC ozone

To evaluate a potential bias in the SPARC ozone data, the SPARC ozone is compared to the SHADOZ and BDBP data in the tropics (Figure 1.2). For reference, the ozone profiles obtained from ERAI are also illustrated. All datasets show similar vertical distribution, with rapidly increasing ozone concentration above 14 km. The data, however, notably differ in the TTL. Specifically, the SPARC ozone has significantly higher ozone concentration in the TTL (15–19km), but a lower ozone concentration in the troposphere compared to the SHADOZ ozone and the BDBP ozone. This is true not only in the deep tropics (Figure 1.2a) but also in the subtropics (Figure 1.2b). It is worth noting that the difference between the SPARC ozone and the SHADOZ ozone is not explained by a sampling issue. Figure 1.3 shows a comparison between the SHADOZ ozone and the SPARC ozone sampled at the SHADOZ stations. The result shows notable differences in ozone concentration between the two sets of data, and the difference is significantly larger than the interstation differences in the SHADOZ data.

A quantitatively similar result is also found in the latitude–height distribution of the ozone difference between SPARC and BDBP (SPARC–BDBP; Figure 1.2c). This comparison reveals that the SPARC ozone has ~30% higher

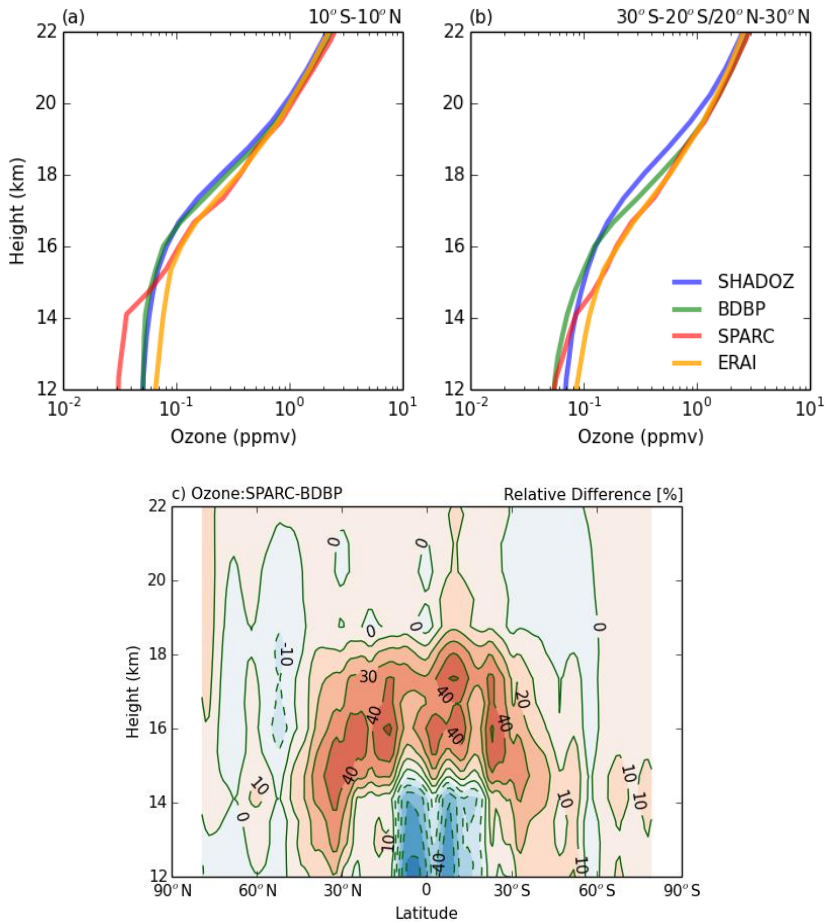


**Figure 1.2.** Ozone profiles from the SPARC, SHADOZ, BDBP and ERAI in the (a) deep tropic (10°N−10°S) and (b) subtropics (30°S−20°S and 20°N−30°N). (c) Latitude-height structure of relative ozone difference between the SPARC and BDBP datasets (SPARC – BDBP). Note that ozone mixing ratio is shown in log scale (unit is ppmv; upper panels), and the relative difference (shown in %) is computed as 100 × ($O_3^{SPARC}$ – $O_3^{BDBP}$) / 0.5× ($O_3^{SPARC}$+ $O_3^{BDBP}$).

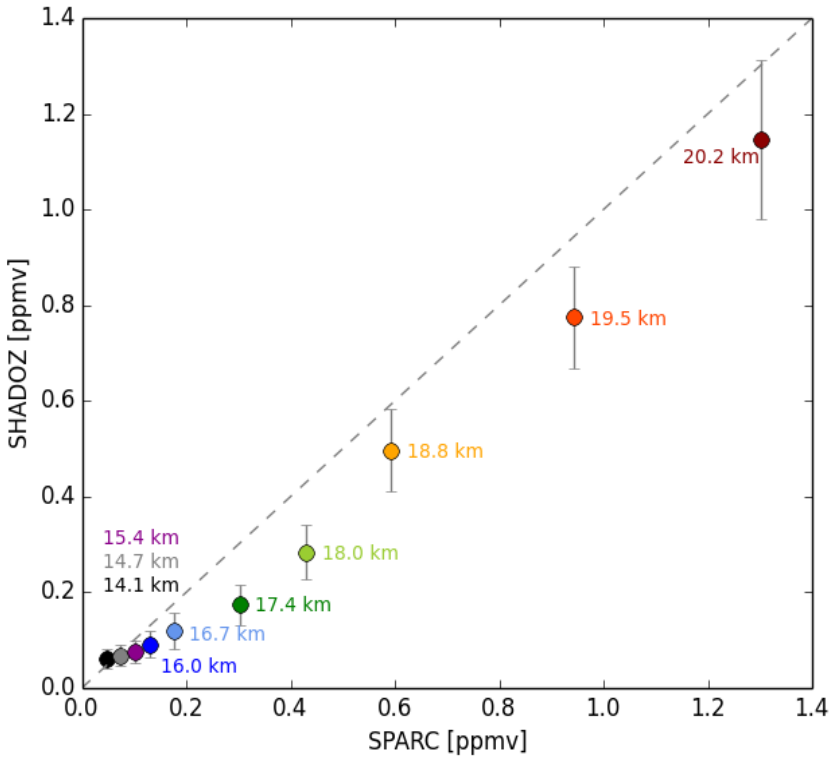


**Figure 1.3.** Scatter plot of SPARC ozone data against the SHADOZ observation in the TTL. The SPARC data is sampled at the locations of 13 SHADOZ stations. The circles and error bar present mean and standard deviation of the values from different station. Colors of the circles denote sampled level of the data.

ozone concentration in the TTL (30°S–30°N; 14–18 km), with a maximum difference of up to ~50%.

The mismatch between the SPARC ozone and the SHADOZ (or BDBP) ozone is likely caused by the characteristics of the chemistry-climate models used for the SPARC ozone production (CAM3.5 and GISS-PUCCINI). Since the ozone concentration in the TTL is influenced by various processes such as convection (e.g., Folkins and Martin, 2005) and large-scale vertical transport (e.g., Fueglistaler et al. 2011; Abalos et al. 2013) in the tropics, as well as lateral mixing processes in the subtropics (e.g., Ploeger et al. 2012), simulated ozone concentration in a chemistry-climate model can be sensitive to the transport characteristics of the model (e.g., Hardiman et al. 2015). In fact, chemistry-climate models included in the CCMVal2 project exhibit pronounced intermodel spread in TTL ozone concentration (Gettelman et al. 2010). These uncertainties in the modelled ozone could be the cause of the discrepancy between the observation and the modelled ozone in the TTL.

The temperature difference between the SOZ and CTR runs (Figure 1.5a) shows an almost opposite pattern to the temperature bias in the CTR run (Figure 1.1a). The experiment with the BDBP ozone (Figures 1.1c and 1.4b) shows a weaker improvement, but also shows similar temperature changes as for SOZ in the TTL and lower stratosphere. The TTL warm bias is reduced by up to ~1 K. This result

suggests that the change in tropical ozone has a strong impact on the thermal structure in the TTL and lower stratosphere.

In order to test the local impact of the TTL ozone, additional experiments are conducted by isolating the ozone change within the TTL region. In these tests (SOZ_TTL and BDBP_TTL runs), either the SHADOZ or BDBP ozone is prescribed only in the TTL (14–20 km, 30°S–30°N) and the SPARC ozone is used in the other regions. Figures 1.1d and 1.1e present the temperature biases in these experiments. They show the same results as those obtained for the SOZ and BDBP runs. This indicates that most improvements in the TTL temperature biases are caused by the correction of ozone bias in the TTL.

### 1.3.3. Temperature budget analysis

The thermal budget is further examined in the tropics (30°S–30°N) for radiation, advection and residual terms for CTL, SOZ and BDBP (Figure 1.4). The advection term includes resolved horizontal and vertical circulation, while the residual term includes model diffusion and parameterizations (convection, microphysics and vertical mixing processes). As discussed above, the thermal budget in the TTL is mainly balanced by radiative heating and dynamical cooling (mostly by upwelling). Also, negligible cooling by the residual term exists in the TTL, largely due to the vertical mixing processes (the non-local mixing process largely contributes to this term). A marked difference between SOZ and CTL is found in the TTL. The SOZ experiment shows less radiative heating which is balanced by weaker dynamic cooling in the TTL, indicating that the decreased ozone in the TTL leads to local radiative cooling. A similar response is observed in BDBP, which is slightly weaker compared to SOZ. The difference between SOZ and BDPB is largely due to the difference in ozone in the subtropical TTL, which is prominent at ~18 km (Figure 1.2b).

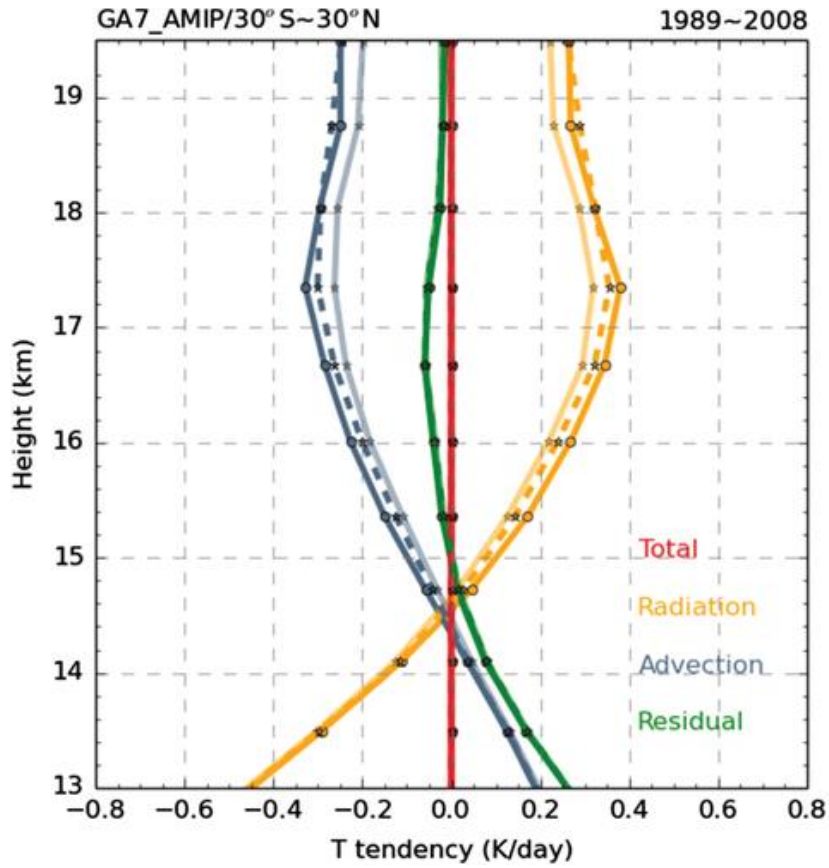


**Figure 1.4.** Heating rates (K/day) for radiation (longwave and shortwave; yellow), dynamics (advection by resolved horizontal and vertical circulations; grey), and residual (model numerics and subgrid-scale parameterizations; green) terms averaged over the tropics (30°S–30°N). Dark, dashed and light curves indicate CTR, BDBP and SOZ, respectively.

### 1.3.4. Remote response by tropical ozone forcing

The simulations used in this study do not include interactive chemistry; thus, no feedback process with ozone (e.g., Fueglistaler et al. 2011; Ming et al. 2017) is observed. However, it is worth noting that the effect of the ozone change in the TTL also has a remote response in the stratosphere. In the tropics, the cold bias in the lower stratosphere (10–50 hPa in Figure 1.1a) is significantly reduced in the SOZ and SOZ_TTL runs (Figure 1.5a–c). This is largely due to the increase of the terrestrial outgoing longwave radiation that reaches the stratosphere as the ozone absorbs less outgoing longwave radiation in the TTL. In addition, a slight improvement is found in the extratropical lower stratosphere, especially in the Southern Hemisphere. The broad cold anomaly found in the Antarctic lower stratosphere and tropopause layer (Figure 1.1) reduces significantly in these regions. This impact is likely caused by circulation change in the lower stratosphere due to tropical ozone forcing. The local and remote radiative forcing could modify the structure of the Brewer-Dobson circulation in the stratosphere by modifying the background state (and wave guide); this secondary circulation response could contribute to reducing the extratropical temperature biases. The detailed processes will be further tested in a future study.

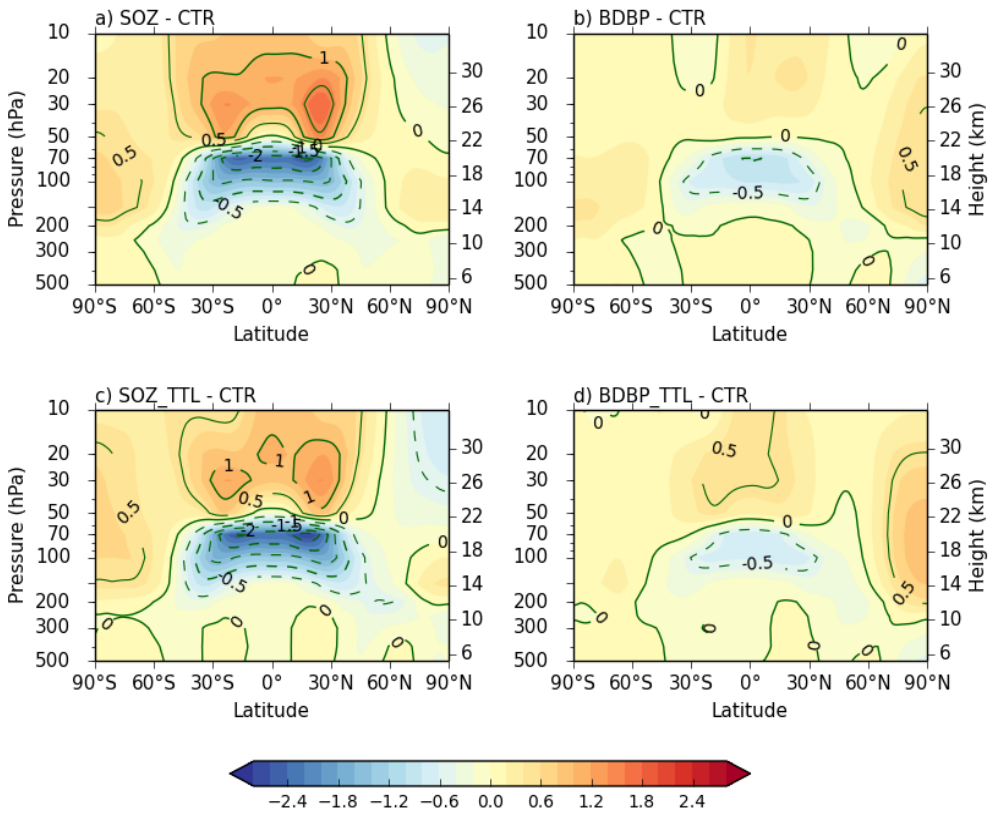


**Figure 1.5.** Longitude-pressure distributions of temperature difference between CTR and other ozone experiments: (a) SOZ, (b) BDBP, (c) SOZ_TTL, and (d) BDBP_TTL. Shading and contour interval are 0.2 K and 0.5 K.

# 2. Influence of UTLS ozone on the QBO-MJO connection

## 2.1. Introduction

The Madden-Julian Oscillation (MJO, Madden and Julian, 1971, 1972) is a dominant mode with dipole convection modes, enhanced and suppressed convection repeatedly from Indian Ocean to western Pacific area in the tropical troposphere. It has the cycle of approximately 30–60 days. The circulation and convection associated with the MJO interact with the global weather and climate system and hence it is considered as a leading source to improve the Subseasonal-to-Seasonal (S2S) prediction skill (Vitart et al. 2017) not only in the tropics but also mid- and high-latitude by teleconnection (Kim et al. 2018; Zhang, 2005, 2013).

Previous studies showed that MJO convective activity appears differently depending on the phase of equatorial stratospheric Quai-Biennial Oscillation (QBO) in the boreal winter (Martin et al. 2021; Son et al. 2017; Yoo and Son, 2016). In particular, when the zonal wind anomaly is an easterly phase (EQBO) in the lower stratosphere, MJO convection tends to be active and conversely suppressed with a westerly phase (WQBO). The eastward propagation speed of the MJO in the EQBO period is slower, the duration is longer than the WQBO period. It tends to move to the western Pacific region. Lim et al. (2019) and Kim et al. (2019) showed that prediction skill during the EQBO period is higher by roughly 10 days than that of

the WQBO with many dynamical models such as S2S and climate models (e.g., CMIP5 and 6). However, the precise mechanisms which can be explain the causal relationship are still not well understood.

Among others, many studies have suggested that QBO-induced static stability changes in the upper troposphere and lower stratosphere (UTLS) is a driver QBO-MJO relationship (Hendon and Abhik, 2018; Martin et al. 2019; Nie and Sobel, 2015; Son et al. 2017). The lower stratosphere is cooled by the secondary circulation during the EQBO based on the 50-hPa zonal wind in the tropics, which reduces the static stability in the UTLS region. Simultaneously, the height of tropopause increases and therefore the deep convection associated with the MJO can reach higher altitude, increasing the possibility of the QBO-MJO interaction.

QBO-induced thermal stratification and the tropopause change can be further enhanced by the diabatic process associated with water vapour or ozone change as well as by adiabatic process. Specifically, cloud–radiation feedback (Lim et al. 2018; Son et al. 2017; Sakaeda et al. 2020; Sun et al. 2019) and ozone-radiative feedback (Lim and Son, 2020; Raphaldini et al. 2021) can strengthen the UTLS change. For example, cooling near the tropical tropopause results in more cirrus clouds and more longwave heating consequently. This may contribute to weaken the static stability in the UTLS. Moreover, when the ascending motion strengthens by

secondary circulation, low ozone concentration flows into the lower stratosphere from the upper troposphere and therefore the absorption of the shortwave radiation reduces. This weakens the UTLS static stability as the temperature in the lower stratosphere cools. Namely, the cloud-radiative and ozone-radiative feedbacks could contribute to strengthen the MJO convection by reducing the static stability in the UTLS region.

Unlike observation, most climate models do not simulation the QBO-MJO connection (Lim et al. 2020; Kim et al. 2020; Martin et al. 2021). This is because the most models do not simulate the temperature in the UTLS region (Kim et al. 2020). Temperature difference between EQBO and WQBO in observations represents a range of up to about 3 K at 70 hPa, whereas it is quite weak in the models. The physical processes of cirrus clouds and ozone are being discussed. Cirrus processes are not well simulated in many current climate models. Ozone is also not being properly prescribed. Most operational S2S models ignore the ozone–radiative feedback by using the climatology ozone. Although ozone is calculated directly in the chemical climate models, QBO itself is not well simulated (Butchart et al. 2017).

This study aims to evaluate the importance of ozone-radiative feedback in the QBO-MJO connection. Specifically, we examine how the ozone variability could affect the QBO-MJO connection by prescribing the real observed ozone instead of

ozone climatology values. Unlike previous studies, S2S model is used in this study. Since the S2S models have a higher resolution compared to the general climate models, it has the advantage of being able to describe the physical processes in the troposphere and stratosphere in more detail.

## 2.2. Data and Methods

### 2.2.1. Observational datasets

In this study, Stratospheric Water and OzOne Satellite Homogenized (SWOOSH), which is combined the multiple satellite ozone observation such as SAGE-II, III, HALOE, UARS MLS, EOS Aura MLS (Davis et al. 2016), is used. Although SWOOSH ozone has been available since 1984, its spatial and temporal coverages are coarse until 2003. Hence, only the last 17 years (2004–2020) are considered in this study. The SWOOSH ozone at a horizontal resolution of 2.5–degree is used. The SWOOSH ozone is available only for 12 pressure levels ranging from 261 hPa to 1 hPa. In the troposphere, Atmospheric Chemistry and Climate (AC&C)/Stratospheric Processes and their Role in Climate (SPARC) climatological ozone is used.

As a reference, daily zonal wind and temperature from the European Centre for Medium-Range Weather Forecasts (ECMWF) Reanalysis v5 (ERA5, Hersbach and Dee, 2016; Copernicus Climate Change Service, https://climate.copernucus.eu) data are used. The OLR data from National Oceanic and Atmospheric Administration (NOAA) are also used to describe tropical convective activity. These data are utilized to define the QBO phase and MJO index.

### 2.2.2. Evaluation metrics

To sort out the each QBO phases period corresponding the strong MJO amplitude, the standard methods are followed the QBO index in Yoo and Son (2016). Generally, the QBO index is based on the 50-hPa zonal mean zonal wind anomalies integrated over 10°S–10°N. When the QBO index is below -0.5 standard deviation, it is defined as EQBO winter. WQBO winter is when the index is above 0.5 standard deviation.

To calculate the MJO index, the real-time multivariate MJO index (RMM, Wheeler and Hendon, 2004), which is commonly being used is considered. Briefly, the RMM index is generated from 200-hPa (U200) and 850-hPa (U850) zonal winds and outgoing longwave radiation (OLR) averaged over the deep tropics (15°S–15°N). The of of the predicted equatorially average OLR, U850 and U200 anomalies are projected onto the observed EOF, which is the same method used in Marshall et al. (2017).

The OLR distribution is applied the band-pass filter with the period of 20–100 days corresponding to the typical time scale of MJO (Waliser et al. 2009). To filter the longer time scale than 61 days, prescribe observation data for the period prior to the model initialization and put the zero posterior to the period of model prediction. This zero-padding method is usually used to check the intra-seasonal

variability with the short integration time of the S2S models (Janiga et al. 2018; Wheeler and Weickmann, 2001).

### 2.2.3. Model and experimental design

In this study, the GloSea5 is used which is an ensemble prediction system of the UK Met Office as fully resolving stratosphere for monthly to seasonal forecasting based on the Hadley Centre Global Environment Model version 3 (HadGEM3, MacLachlan et al. 2015). This model is fully coupled with atmosphere–land–ocean–sea-ice components. The horizontal resolution for atmosphere is ~0.83 degree of longitude and ~0.56 degrees of latitude. The model has 85 vertical levels with the model top at 0.01 hPa. The atmosphere and land surface are initialized with the European Centre for Medium–Range Weather Forecasts (ECMWF) Interim reanalysis data (ERA-Interim, Dee et al. 2011). For the ocean and sea-ice initializations, the ocean analyses are used from Forecast Ocean Assimilation Model (FOAM). The model outputs are interpolated on the horizontal resolution by 2.5–degree interval. See MacLachlan et al. (2015) for the full details of the GloSea5.

To investigate the impact of ozone-induced static stability change in the UTLS region on the QBO-MJO connection, the initialization date of January 1 2006 is chosen (Figure 2.2). The case corresponds to the period when the observed ozone anomaly is obvious during EQBO period which the sampling of the SWOOSH ozone data is possible onward 2004. Also, it is consistent with the cases used in the previous studies (e.g., Hendon and Ahbik, 2018; Martin et al. 2020). The reference simulation

uses the climatological ozone (COZ) for the period of 2004–2020. The sensitivity simulation is conducted with the target year SWOOSH observation ozone (YOZ). The model integrated for 61 days for each simulation. Apart from the ozone data, all other configurations are identical between COZ and YOZ simulations. Each simulation has three ensemble members, which is generated by perturbing model physics stochastic kinetic energy backscatter.

The operational S2S prediction is similar to the COZ experiment except for ozone data and the prescription cycles. The monthly zonal-mean SWOOSH ozone is interpolated to daily timescale from one month to another in the COZ experiment, while the AC&C/SPARC monthly ozone climatology is prescribed in the operational version of GloSea5.

## 2.3. Results

### 2.3.1. Ozone and temperature distributions in QBO

To examine the zonal-mean zonal wind, ozone and temperature change on the QBO phases, Figure 2.1 shows the time and pressure distributions averaged 10°S–10°N from the period of 2004 to 2020. The equatorial zonal-mean zonal wind regime propagates downward into the lower stratosphere while repeating the easterly and westerly wind as time progresses (Figure 2.1). Generally, westerly anomalies tend to be more regular and rapidly propagated downward with about 20 m $s^{-1}$ above at 50 hPa, but sharply decrease below the level. On the other hand, the easterly anomalies are stronger and have a relatively long duration (Baldwin et al. 2001).

The vertical wind shear anomaly by QBO-induced also affects the temperature by the thermal wind balance (Andrew et al. 1987) (Figure 2.1b). When the easterly wind shear forms in the lower stratosphere during the EQBO period, it induces upward motion and negative temperature anomaly near equatorial UTLS and downward motion and positive temperature anomaly in the subtropical region (Collimore et al. 2003). Therefore, the temperature distribution also shows cold anomalies in EQBO and warm anomaly in WQBO by the adiabatic process related to the vertical motion. It can be affected by diabatic processes such as ozone as well as adiabatic processes associated with circulation.

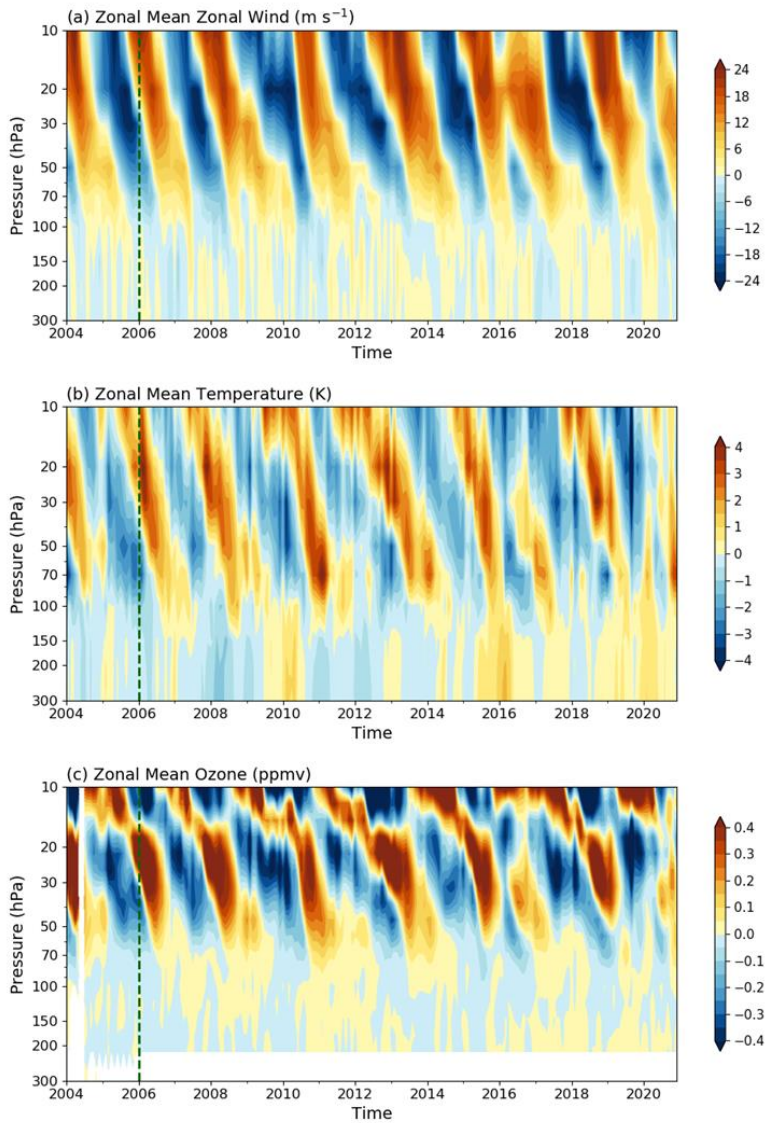


**Figure 2.1.** Time-pressure cross section of (a) monthly zonal-mean zonal wind (m $s^{-1}$), (b) temperature anomalies (K) and (c) ozone (ppmv) averaged over 10°S–10°N.

The QBO-induced vertical shear changes also affect the chemical compositions such as ozone and water vapour. When upward motion is formed in the UTLS region by the secondary circulation in EQBO, air with a low ozone concentration from the upper troposphere flows into the lower stratosphere. During WQBO periods, the ozone concentration in the UTLS region increases as ozone is transferred from the stratosphere to the upper troposphere. Therefore, similar to the QBO pattern of zonal mean zonal wind and temperature, equatorial ozone distribution exhibits positive anomalies with the westerly wind anomalies and negative anomalies with the easterly wind anomalies. It shows downward propagation pattern from the stratosphere to the troposphere by alternating positive and negative anomalies over time (Figure 2.1c). The vertical distribution of ozone over time exists in two layers, the lower and middle stratosphere based on about 20 hPa, which has a quarter phase difference. The chemical lifetime of ozone is short due to photochemical reactions with other gases above 20 hPa, whereas it is considered a long-lived tracer because it is relatively long compared to the dynamic process below 20 hPa (Baldwin et al. 2001).

To examine the spatial distribution of zonal mean zonal wind, temperature and ozone depending on QBO phases, Figure 2.2 shows their anomalies as a function of latitude and pressure for January–February 2006 chosen as a case study. The anomaly was calculated by removing the monthly mean climatology. The zonal mean

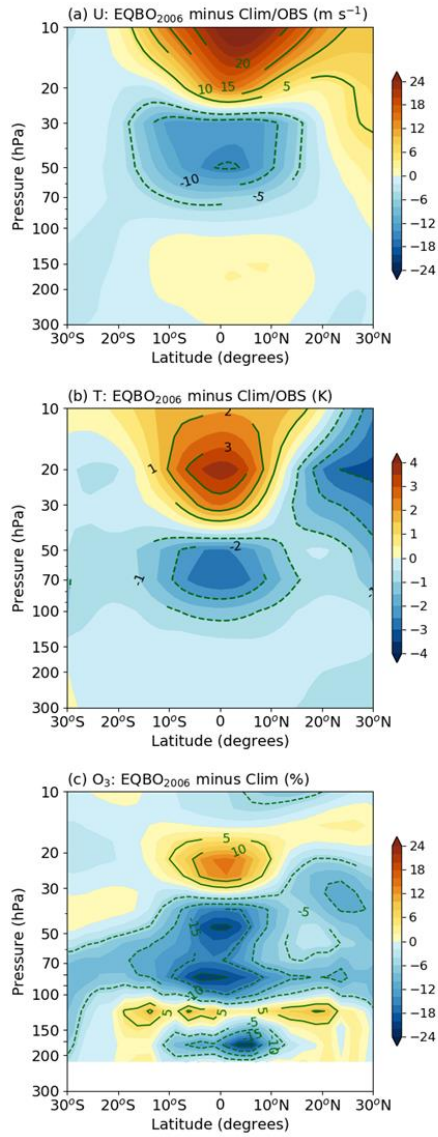


**Figure 2.2.** Latitude-pressure distribution of (a) zonal wind anomalies (m $s^{-1}$), (b) temperature (K) and (c) zonal-mean ozone (%) in EQBO winter of January–February 2006.

zonal wind is ~15 m $s^{-1}$ at the centre of 50 hPa, and the temperature has difference by ~2.5 K based on 70 hPa. This result is similar to the range seen in long-term (1974–2014) observations (see Fig. 4 in Kim et al. 2020). During the EQBO case, tropical ozone concentration is 20–25 % less in 40–100 hPa, and 10–15 % more in 15–30 hPa compared to the climatology. This is because the stratospheric ozone anomalies could be influenced by the anomalous vertical advection on QBO phases (e.g., Baldwin et al. 2001).

### 2.3.2. Temperature difference in the UTLS

Since S2S models adopt different numerical schemes, boundary conditions and resolutions, it is known that the anomaly of QBO zonal wind is a little bit different (Lim et al. 2019; Wang et al. 2019). Realistic simulation of the QBO during the forecast periods in the S2S models play an important role to examine QBO-MJO connection. As a result of comparison with observations for the daily 50 hPa zonal mean zonal wind (U50) for the whole forecast lead time of COZ and YOZ experiments, each correlation was 0.76 and 0.82, respectively. The root mean square errors (RMSE) are also in the range of 2.4–2.9. As shown in Lim et al. (2019), both experiments are well correlated with the observation, even though the RMSE is slightly higher than the multiple cases evaluation.

Since S2S models adopt different numerical schemes, boundary conditions and resolutions, it is known that the anomaly of QBO zonal wind is a little bit different (Lim et al. 2019; Wang et al. 2019). Realistic simulation of the QBO during the forecast periods in the S2S models play an important role to examine QBO-MJO connection. As a result of comparison with observations for the daily 50 hPa zonal mean zonal wind (U50) for the whole forecast lead time of COZ and YOZ experiments, each correlation was 0.76 and 0.82, respectively. The root mean square errors (RMSE) are also in the range of 2.4–2.9. As shown in Lim et al. (2019), both

experiments are well correlated with the observation, even though the RMSE is slightly higher than the multiple cases evaluation.

Figure 2.3 shows the zonal mean zonal wind and temperature anomalies as a function of latitude and pressure compared to the observed climatology for each of the COZ and YOZ experiments from January 1 to February 28, 2006 during the same period as the observation. As mention earlier, the only difference between the two experiments is the prescription of stratospheric ozone. The ozone difference between YOZ and COZ experiments is shown in Figure 2.2c. The zonal mean zonal wind in both experiments show similar structures to observations. The zonal mean zonal wind in COZ shows 1–2 m $s^{-1}$ stronger than that of observation centred on 50 hPa. The difference between the two simulations 0.5 m $s^{-1}$, which is weaker in YOZ experiments.

Both experiments show a cold anomaly in the lower tropical stratosphere of 50–100 hPa, a warm anomaly in the middle stratosphere around 20–30 hPa and a weak warm anomaly in the off-equatorial subtropical lower stratosphere (Figure 2.3 d–f). This is similar to the previous study (Martin et al. 2021) using the ECMWF model. Compared to the observation, both experiments simulate very weak cold anomaly near 70 hPa in the lower stratosphere (comparison with Figure 2.2b). This implies that the temperature change in the lower tropical stratosphere due to EQBO

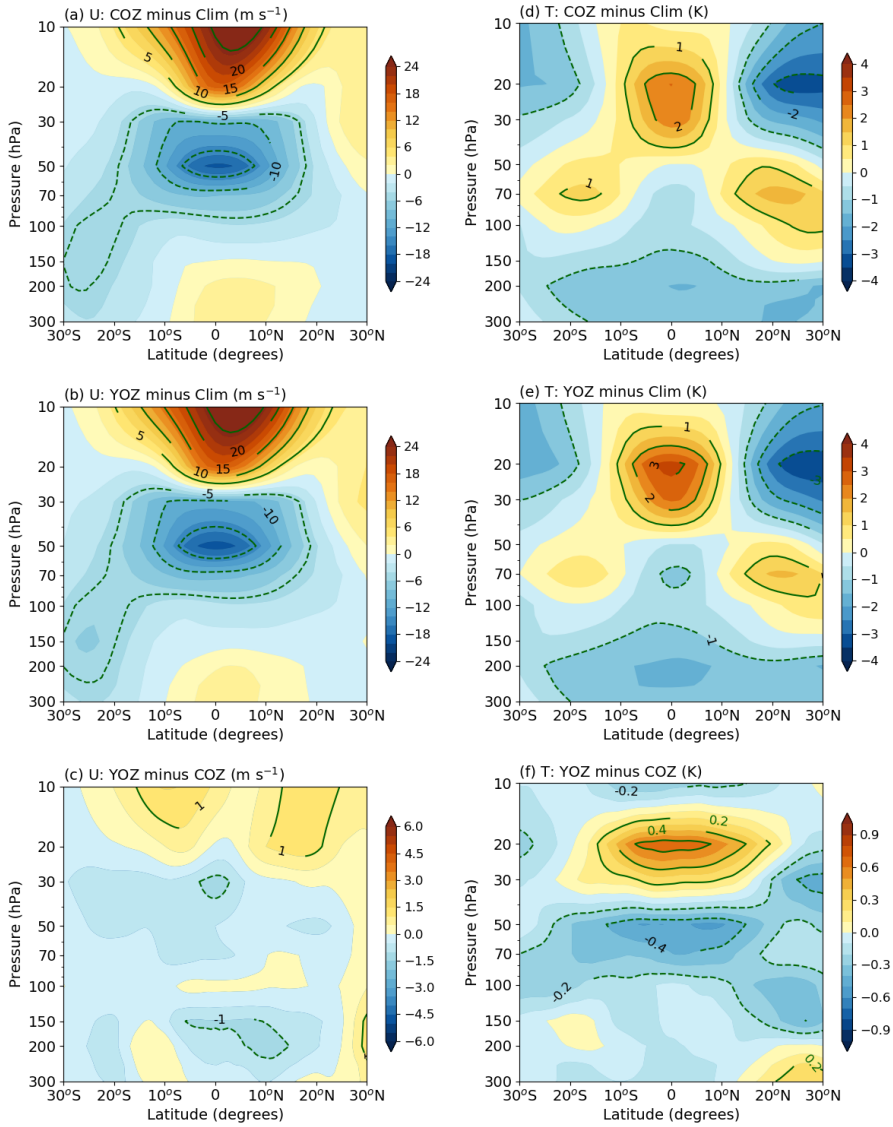


**Figure 2.3.** Differences in zonal-mean zonal wind (m $s^{-1}$) and temperature (K) (a), (d) between COZ and observed climatology, (b), (e) between YOZ and observed climatology, and (c), (f) between YOZ and COZ experiments averaged over January-February 2006.

secondary circulation is greatly underestimated. It is considered as one of the causes of Lee and Klingaman (2018) that QBO-MJO connection does not appear in the model.

However, the temperature difference in the YOZ experiment was larger and wider in the UTLS region compared to COZ. YOZ experiment shows the temperature difference of the range of 0.4–0.5 K near 50–70 hPa. Previous studies (Butchart et al. 2003; Li et al. 1995; Pohlmann et al. 2019; Tweedy et al. 2020) have shown that when the interactive chemical process including ozone is considered in the model, heating and cooling of diabatic process by ozone can intensify the temperature anomaly of QBO by about 15–30 % compared to those which did not. The result is consistent with the previous study, which the radiation process by observed ozone could strengthen the temperature anomaly by about 17 % compared to the climatology.

In order to examine the zonal mean temperature change as function of forecast lead time in the COZ and YOZ experiments, Figure 4 shows the longitude and time distributions of zonal mean temperature averaged from 15°S to 5°N in January 1 to February 28, 2006. Figure 4a–c show the observation, COZ and YOZ experiments, respectively. The difference between the two experiments (YOZ minus COZ) is in Figure 4d. It is clear that the positive anomaly at the centre of 20 hPa and

the negative anomaly at the centre of 70 hPa in the observation. It can be seen that the cold anomaly is strengthened around February 1 at the center of the 70 hPa. In both experiments, the temperature anomaly near 20 hPa was somewhat similar to that of the observation, however, the anomaly is weakly simulated compared to the observation. Also, the cold anomaly at 70 hPa is not well simulated. The initial cold anomaly disappeared within 10 days and there is no apparent temperature anomaly beyond that. Contrary to observation, there is a strong cold anomaly in the upper troposphere below 100 hPa. This suggests serious defect in the UTLS process in the model.

YOZ shows a large temperature difference between 50–70 hPa and 20 hPa compared to COZ. In particular, the anomaly difference between the two experiments reaches the maximum from January 20 to February 1, which is about 20 days after initialization. This implies that the radiative time scale is around 20 days in the lower stratosphere (Randel et al. 2021).

### 2.3.3. MJO response

To investigate the MJO response to the static stability change in UTLS (Figure 2.4d), OLR distributions with the 20–100 days band-pass filter applied to observation and experiments examine as a function of longitude and time (Figure 2.5). The observation values are used in the period prior to the model initialization and the zero value is prescribed posterior to the forecast lead time (Janiga et al. 2018).

Convection starts in the western Indian ocean around 30–60°E and develops gradually. While maintaining its intensity, it moves slowly eastward from the Indian ocean to the Pacific Ocean during the forecast lead time. On the other hand, the MJO propagation pattern is simulated qualitatively well, but the strength of convection related to the MJO is underestimated in the COZ and YOZ experiments. Similar to the observation, the development of convection begins near the western Indian Ocean, but the convection is getting weaken in the Indian ocean near 60–90°E and the Maritime Continent near 120°E. However, the difference between two experiments is very small in the intensity of convection during the period in which the difference in thermal stratification between the COZ and YOZ experiments is most evident. This is not sensitive in each of the ensemble member. This suggests that the static stability change in the UTLS due to ozone-radiative feedback does not significantly affect the MJO convection. It is presumed that the

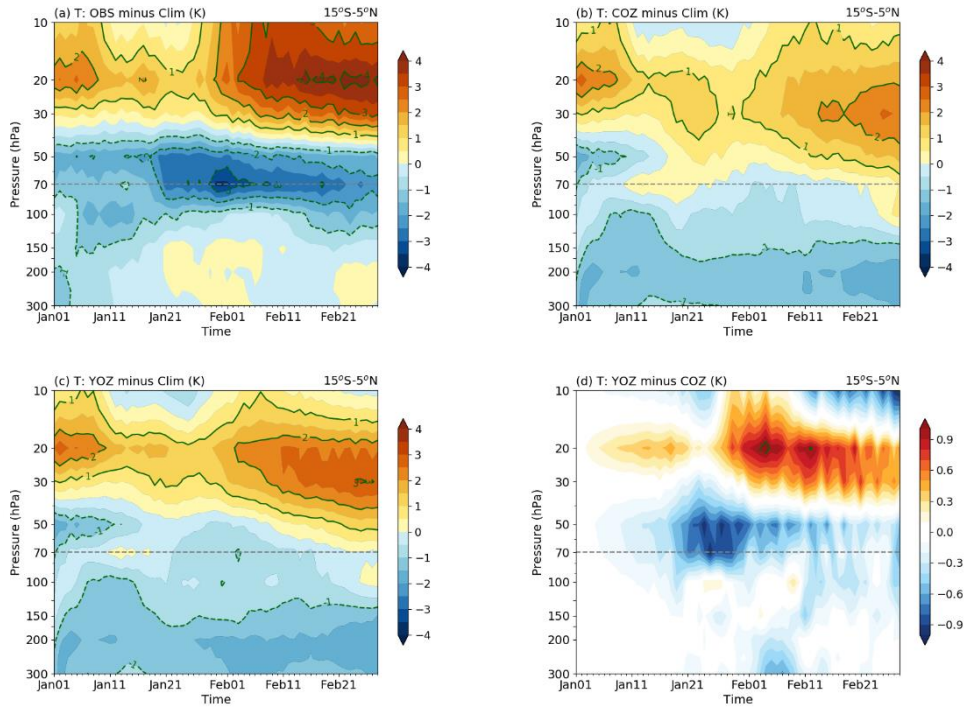


**Figure 2.4.** Longitude-time sections of zonal-mean temperature (K) averaged from 15°S to 5°N in (a) observation, (b) COZ, (c) YOZ, and (d) their difference in January−February 2006

temperature response by ozone-radiative feedback is not large (Figure 2.4d).

To quantitatively examine the difference in amplitude for each phase of MJO, Figure 2.6 shows a standard RMM phase diagram that provides information on the phase and amplitude of MJO over time. The period shown in the figure is from January 8 to February 5 after one week of initialization in which the temperature difference in 50–100 hPa occurs between the two experiments. Each dot means the phase and amplitude of the daily MJO. Each color represents the observation (black), COZ (green) and YOZ (red) experiments, respectively. The MJO convection originating in the east Indian Ocean (MJO phase 3) propagates through the Maritime Continent region (MJO phase 4–5) to the Pacific region in the observation. However, simulated MJO convection, which is significantly weaker than that of the observation, appears in the vicinity of the east Indian Ocean and propagates across the Maritime Continent. When checking the change in RMM, the MJO amplitude difference between the COZ and YOZ experiments is not evident in the period—January 21 to February 1—in which the static stability change reaches the maximum in the UTLS. This result is consistent with Figure 2.5.

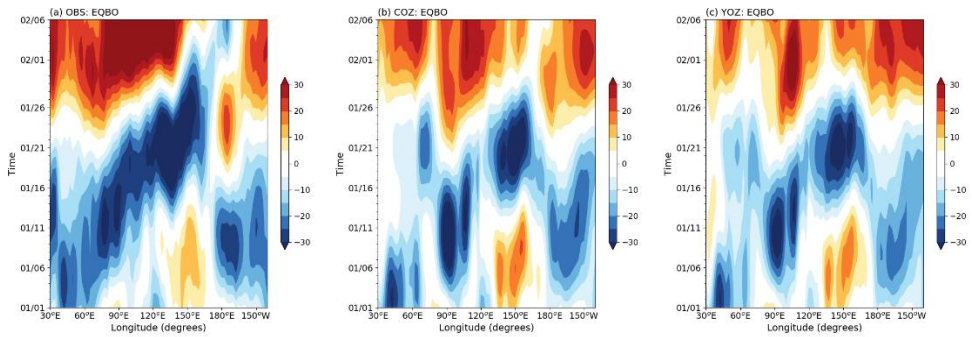


**Figure 2.5.** Longitude-time sections of bandpass-filtered (20–100 days) OLR (W m$^{-1}$) averaged from 15°S to 5°N in (a) observation, (b) COZ, (c) YOZ and (d) the difference between YOZ and COZ. Temporal evolution is shown from 1 January to 6 February, 2006 when MJO is well defined in observation.

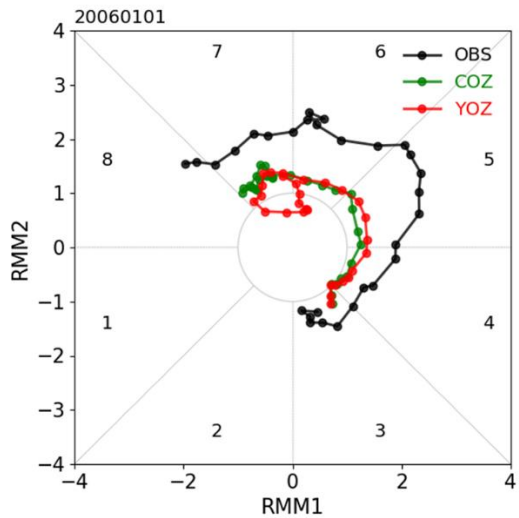


**Figure 2.6.** MJO RMM phase diagram in observation (black), COZ (green), and YOZ (red). The time evolution starts on 8 January and ends on 5 February, 2006.

# 3. Impact of stratospheric ozone on the subseasonal prediction in the Southern Hemisphere spring

## 3.1. Introduction

Stratosphere–troposphere coupling, associated with the polar vortex variability, is a prominent dynamical process in the extratropics. In the Southern Hemisphere (SH) (Baldwin et al. 2003; Byrne et al. 2018; Hio and Yoden, 2005; Lim et al. 2018; Seviour et al. 2014; Thompson et al. 2005), such downward coupling occurs in the austral spring and significantly modulates the zonal mean circulation in the troposphere as evidenced in the southern annular mode (SAM). As such, it has been considered as one of the most important sources of tropospheric predictability on the subseasonal-to-seasonal (S2S) timescale. Seviour et al. (2014) and Byrne et al. (2019), for instance, showed that a significant prediction skill of the SAM re-appears in early October after a period of no prediction skill in their model simulations. This skill re-emergence has been attributed to the polar vortex variability and its downward influence (Seviour et al. 2014). The models which have participated in the S2S prediction project (http://s2sprediction.net) also show an enhanced prediction skill in early October, although the skill re-emergence is not always statistically significant (not shown).

It is well documented that stratospheric ozone (hereafter referred to as

ozone unless otherwise specified) undergoes substantial interannual variation (e.g., Salby et al. 2011; Son et al. 2013). This ozone variation can affect the polar vortex and its downward coupling. Son et al. (2013) showed that September polar ozone anomaly is significantly correlated with October SAM on interannual time scale: The chances of hot and dry weather in southern Australia are increased when polar stratospheric ozone is anomalously high in the austral spring. However, their result does not necessarily indicate that ozone anomaly is a driving factor for the tropospheric circulation change, as the ozone anomaly itself is primarily determined by the polar vortex. In general, strong upward propagating waves act to weaken and warm the polar vortex in the late winter. The associated meridional circulation transports ozone from low latitudes to the pole, increasing ozone concentration over the Antarctic stratosphere in late winter to early spring (Lim et al. 2018; Salby et al. 2011; Shaw et al. 2011; Solomon, 1999). The increased ozone concentration then can further weaken the polar vortex through an increased shortwave radiative heating and possibly enhance the downward coupling. This vortex-ozone relationship is well observed during stratospheric sudden warming events. In 2002 and 2019 spring when the polar vortex broke down, total column ozone (TCO) has sharply increased (Hendon et al. 2020; Lim et al. 2019; Son et al. 2013).

Although the ozone radiative feedback could help strengthen the downward coupling, by modulating the polar vortex, its relative importance against the dynamic coupling has only recently been examined. Hendon et al. (2020) showed that

prescribing the observed ozone during the 2002 SH sudden warming event—when ozone was anomalously plentiful over the polar cap in the SH—can facilitate the vortex weakening via radiative heating and enhance the surface response (negative SAM) in October in their model simulation. Yook et al. (2020) more generally showed that interactive ozone acts to increase stratospheric variability. Although they did not discuss its impact on tropospheric predictability, they showed that interactive ozone enhances the persistence of stratospheric variability, from which it can be inferred that it also acts to increase predictability of the stratosphere and possibly the troposphere. These results suggest that a realistic ozone could improve the S2S prediction in the SH in October–November when the downward coupling is prominent. However, most operational S2S prediction models use zonally and monthly averaged climatological ozone and hence ignore its year-to-year variation (Domeisen et al. 2020).

In this study, we evaluate the impact of year-to-year varying ozone in the S2S prediction using the Global Seasonal Forecasting System version 5 (GloSea5, MacLachlan et al. 2015). To extend and generalize Hendon et al. (2020), multi-year model experiments are conducted. Specifically, the two sets of reforecast experiments are carried out by prescribing either climatological ozone or year-to-year varying ozone for the period of 2004–2020. As shown below, the reforecasts with time-varying ozone show an improved prediction skill in October, compared to those with climatological ozone.

## 3.2. Data and method

### 3.2.1. SWOOSH ozone data

Stratospheric Water and OzOne Satellite Homogenized (SWOOSH, http://csl.noaa.gov/groups/csl8/swoosh) ozone database are combined product with the multiple satellite observations including Stratospheric Aerosol and Gas Experiment (SAGE)-II and III, Halogen Occultation Experiment (HALOE), UARS MLS, and EOS Aura MLS from 1984 (Davis et al. 2016). This data is available for 12 pressure levels ranging from 261 hPa to 1 hPa (difference the beginning level for water vapor) with zonal-mean monthly-mean time series. This merged data is provided with the different horizontal resolution, 2.5°, 5° and 10° zonal-mean grids based on the pressure and isentropic vertical levels.

Although SWOOSH ozone has been available since 1984, its spatial and temporal coverages are coarse until 2003. Hence, only the last 17 years (2004–2020) are used. In all the experiments, monthly SWOOSH data are interpolated into daily timescales in chapter 3.

### 3.2.2. Model description

The GloSea5, which is the operational ensemble seasonal prediction system

of the UK Met Office (MacLachlan et al. 2015), is used in this study. This model became operational in January 2014 as the joint seasonal prediction system of the UKMO and its partner the Korea Meteorological Administration. The GloSea5 is fully coupled with atmosphere–land–ocean–sea ice components. The horizontal resolution of the atmosphere is ~0.83 degrees of longitude and ~0.56 degrees of latitude. In the vertical, a total of 85 levels with the model top at 0.01 hPa are used. The ocean and sea ice are initialized with the Forecast Ocean Assimilation Model Ocean Analysis (Blockley et al. 2014). The atmospheric and land surface initial conditions are obtained from the European Centre for Medium-Range Weather Forecasts (ECMWF) Interim reanalysis data (ERA-Interim, Dee et al. 2011) for the period of 2004–2016. After 2017, the initial conditions are taken from the analysis of the KMA/UKMO numerical weather prediction data assimilation system. See MacLachlan et al. (2015) for the full details of the GloSea5.

### 3.2.3. Experimental Design

A monthly zonally averaged ozone climatology is prescribed in the model. As a default, the Atmospheric Chemistry and Climate (AC&C)/Stratospheric Processes and their Role in Climate (SPARC) ozone for the period of 1994–2005 is used in the operational mode. In this study, the latest ozone data from the Stratospheric Water and OzOne Satellite Homogenized (SWOOSH) ozone at a horizontal resolution of 2.5° are used. These data com bine the multiple satellite observations such as SAGE-II and III, HALOE, UARS MLS, and EOS Aura MLS observations (Davis et al. 2016). Since SWOOSH ozone is available only for 12 pressure levels from 261 to 1 hPa, it is combined with AC&C/SPARC ozone below 261 hPa and above 1 hPa.

All experiments are initialized on September 1st of each year for the period of 2004–2020 and integrated for 61 days. Although SWOOSH ozone is available since 1984, its spatial and temporal coverages are coarse until 2003. Hence, only the last 17 years (2004–2020) are considered in this study. Because of the limitation of computing resources, only 18 ensemble members are used. In all reforecasts, the monthly zonal mean SWOOSH ozone is interpolated to daily timescale in order to allow a smooth transition from one month to another. In the operational version of GloSea5, ozone is prescribed on the 360-day calendar. This could lead to radiative

heating or cooling errors in the polar regions in the spring when the ozone concentration changes rapidly (Hendon et al. 2020). In this study, we prescribe ozone data based on the Gregorian calendar and update it every day.

Here, it should be emphasized that only the zonal mean ozone is considered in this study. It has been reported that the zonally asymmetric ozone distribution can affect the zonal mean circulation in both the stratosphere and troposphere (e.g., Rae et al. 2019). However, three-dimensional ozone distribution is not considered in this study as the zonally averaged ozone is prescribed in the operational GloSea5. More importantly, the ozone datasets used in this study, i.e., AC&C/ SPARC and SWOOSH ozone, are available only for the zonal mean value.

The two sets of experiments are conducted with different stratospheric ozone concentrations. The reference run prescribes the climatological zonal mean SWOOSH ozone (COZ), while the sensitivity run uses the year-to- year varying zonal mean SWOOSH ozone (YOZ) for 17 years. Except for the interannual variation of stratospheric ozone above 261 hPa and below 1 hPa, all other configurations are identical between the two experiments. Note that COZ ozone is derived for the period of 2004–2018. This causes a subtle difference of YOZ ozone climatology from COZ ozone as the former includes the recent two years (i.e., 2019 and 2020).

### 3.2.4. Prediction skill metrics

The reference meteorological fields for model evaluation, such as geopotential height and surface air temperature, are obtained from the fifth generation of the ECMWF atmospheric reanalysis (ERA5, Hersbach and Dee, 2016; Copernicus Climate Change Service, 2017; https://climate.copernicus.eu). The extratropical circulation is quantified by the polar cap index (PCI). The PCI is defined as the geopotential height anomaly integrated south of 60°S at every level in the vertical (Kolstad and Charlton-Perez, 2010) as follows:

$$Z_{PCI} = \frac{\sum \cos\phi \, (Z - \bar{Z})}{\cos\phi}$$

where $Z$ is the geopotential height, $\bar{Z}$ is its climatological mean and $\phi$ is the latitude.

Since the PCI well corresponds to the SAM index not only in the troposphere but also in the stratosphere (Baldwin and Thompson 2009), it is a useful metric to diagnose polar cap stratospheric variability and its downward coupling to the troposphere. There are two common methods to define the SAM index: Principle component (PC) analysis and Gong and Wang method (more detail information related to the SAM index in Ho et al. 2012). The PC analysis is the first PC of empirical orthogonal functions with some variables (e.g., geopotential height, mean

sea level pressure or temperature). Another is simply defined as the normalized zonal-mean sea level pressure difference between 40°S and 65°S:

$$SAM_{Gong\&Wang} = P^*_{40°S} - P^*_{65°S}$$

The model prediction skill is quantified by computing the temporal anomaly correlation coefficient (ACC) between GloSea5 ensemble mean prediction and ERA5. The ACC is defined as follows:

$$ACC(\tau) = \frac{\sum_{i=1}^{n}(f_{i,\tau} - \overline{f_\tau})(O_{i.\tau} - \overline{O_\tau})}{\sqrt{\sum_{i=1}^{n}(f_{i,\tau} - \overline{f_\tau})^2}\sqrt{\sum_{i=1}^{n}(O_{i,\tau} - \overline{O_\tau})^2}}$$

where *i* is the year, n is the total number of years (n = 17), and τ is the forecast lead time from τ=0 to τ=61 days. The ensemble mean prediction and ERA5 are denoted with f*i* and O*i*, respectively. Overbar indicates the time mean over 17 years. In general, ACC decreases rapidly with the forecast lead time. A statistically significant ACC is typically shorter than 2 weeks in the troposphere but over 20 days in the stratosphere (Mariotti et al. 2018; Son et al. 2020).

The significance of ACC is tested by a nonparametric bootstrap method (Goddard et al. 2013; Smith et al. 2013; Wilks, 2006). This method is widely used in the seasonal- to-decadal prediction when the sample size is limited. We randomly

select 17 years from reanalysis and ensemble mean forecasts and then calculate ACC at each lead time. By repeating this process 1,000 times by allowing overlapping selection, a probability distribution of ACC is constructed. The *p*-value is defined as the ratio of negative value from bootstrap-generated 1,000 ACCs on the basis of a one-tailed test of the hypothesis that ACC is greater than 0. If *p*-value is smaller than 0.05, the prediction skill is determined to be statistically significant at the 95% confidence level.

To evaluate the statistical significance of the YOZ-COZ skill difference, the same approach is applied to ACC difference (YOZ minus COZ). The ratio of negative value from bootstrap-generated ACC differences serves as the *p*-value (Goddard et al. 2013).

The significance of ACC difference is also tested using the method proposed by Steiger (1980) and Siegert et al. (2017). As statistical test for detecting improvement in correlation skill, they strongly recommended using the test statistics $T_2$ for comparative studies of correlation skill. They presented the test statistic $T_2$ between two correlation coefficients that share a common variable such as $r_{YOZ}$ and $r_{COZ}$ in this study. If $r_{YOZ}$ has higher value than $r_{COZ}$, the test statistic $T_2$ become large because $T_2$ is proportional to the difference of $r_{YOZ}$ and $r_{COZ}$.

$$T_2 = (r_{YOZ} - r_{COZ}) \sqrt{\frac{(n-1)(1 + r_{(YOZ,COZ)})}{2\left(\frac{n-1}{n-3}\right) R + \frac{1}{4}(r_{YOZ} + r_{COZ})^2 (1 - r_{YOZ,COZ})^3}}$$

$$\mathrm{R} = \left(1 - r_{COZ}^2 - r_{YOZ}^2 - r_{YOZ,COZ}^2\right) + (2 r_{COZ} r_{YOZ} r_{YOZ,COZ})$$

That is, if the calculated $T_2$ is greater than 1.761 (when the number of validation years is 17), $\Delta r$ is interpreted as statistically significant.

## 3.3. Results

### 3.3.1. Ozone interannual variability

We compare the interannual variability of total column ozone using the reanalysis data for seven latitude bands: 90–60°S, 60–30°S, 30–10°S, 10°S–10°N, 10–30°N, 30–60°N, 60–90°N in Figure 3.1. Each ozone band shows the interannual variation. Compared to other regions, the greatest ozone variability appears in the polar region of over the 60°S. There is also a large ozone difference between the high latitude and middle latitude in the SH region.

Figure 3.2a shows the interannual standard deviation of the polar-cap-averaged ozone at 10 hPa for the period of 2004–2020. Here ozone concentration is averaged only over 60°S–90°S weighted by the cosine of the latitude. Its variability is more significant in high latitudes than in low latitudes (Figure 3.2b). As documented in previous studies (Salby et al. 2011; Son et al. 2013), Antarctic stratospheric ozone undergoes significant interannual variation in the late winter and early spring (July to September). Such a substantial variability, largely caused by vertically propagating planetary-scale waves from the troposphere in the austral winter (e.g., Salby et al. 2011), is not limited to the lower stratosphere but extends to the upper stratosphere (not shown). Figure 3.2b illustrates the latitude-pressure distribution of the interannual standard deviation of the September ozone. As a reference, the long-term climatology is overlaid with colored contours. The inter-

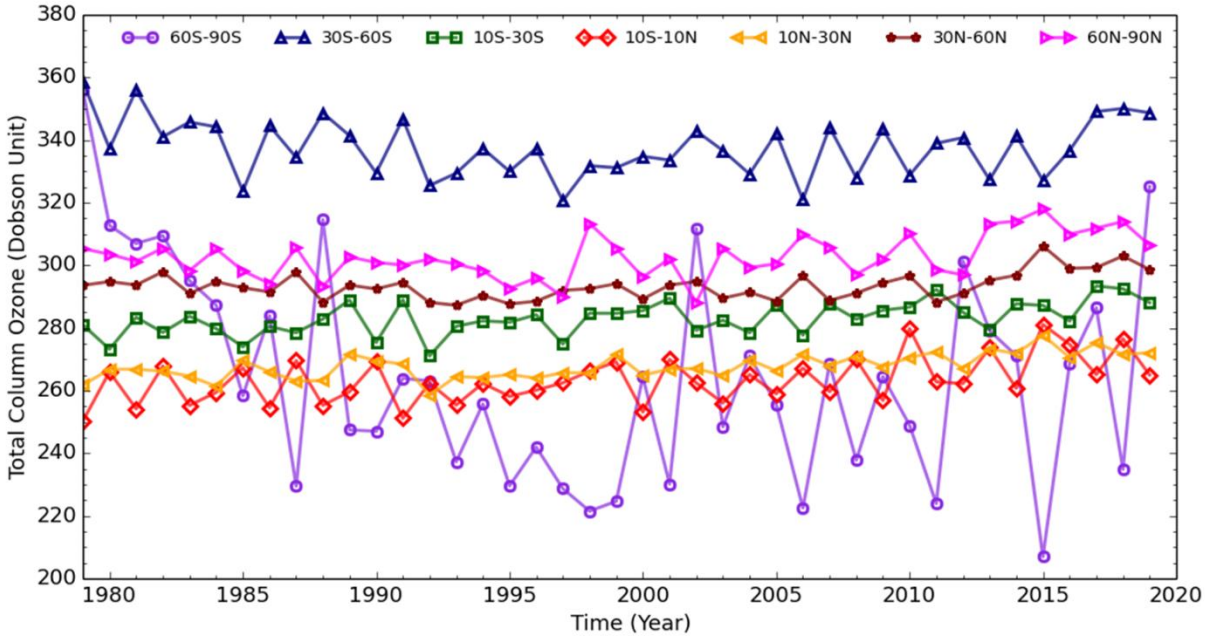


**Figure 3.1.** Annual mean total column ozone (Dobson) for seven latitude bands: 90–60°S (light purple), 60–30°S (navy), 30–10°S (green), 10°S–10°N (red), 10–30°N (yellow), 30–60°N (brick), 60–90°N (magenta).

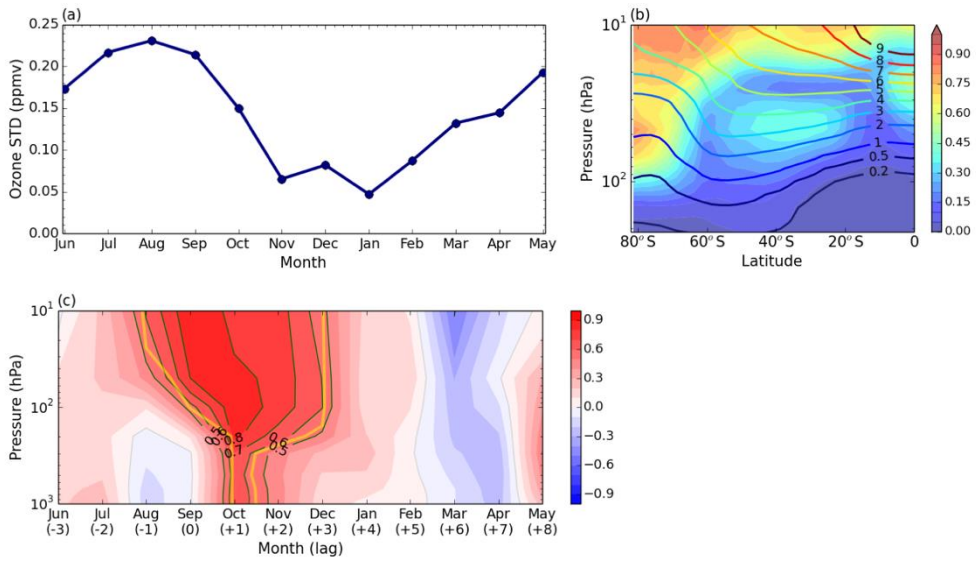


**Figure 3.2.** (a) Interannual standard deviation of 10-hPa Antarctic polar-cap-averaged ozone as a function of the month, and (b) latitude-pressure distribution of interannual standard deviation of September ozone for the period of 2004–2018. The colored contours in (b) denote the climatological ozone mixing ratio in ppmv. (c) Time-pressure distribution of lag correlation coefficients between September 10-hPa polar-cap-averaged ozone and monthly polar-cap-averaged geopotential height anomalies (Polar Cap Index; PCI) for the period of 2004–2018. Contour interval, starting from 0.5, is 0.1, and the values which are statistically significant at the 95% confidence level are denoted with the yellow line.

-annual variability of September ozone at 10 hPa approximately accounts for 20 % of its climatology. An even larger value is observed in the lower stratosphere.

Unlike the observation, ozone forcing in model simulation use the climatology ozone, which is the constant value in each month. Since the prescribed ozone—zonal mean monthly mean—does not reflect the ozone variability (Figure 3.3), it can be underestimated or overestimated the real ozone. Also, the prescribed ozone ignores the zonal asymmetric distribution. Most operational centres use the climatology due to computational burden and resource issues. It definitely could lead to model biases and decrease the prediction skills.

A strong interannual variability of springtime stratospheric ozone is significantly linked to the tropospheric circulation changes (Son et al. 2013). To address such a downward relationship, Figure 3.2c depicts the time-pressure evaluation of lagged correlation coefficients between the September ozone at 10 hPa and monthly-mean PCI at all levels as a function of the month. This figure is similar to Figure 2 of Son et al. (2013) but presents the relationship only in the recent 15 years (2004–2018). The simultaneous correlation coefficient at 10 hPa is 0.88. This indicates that the interannual variability of stratospheric ozone is associated with more than 77% of the interannual variability of polar vortex in September. This strong correlation extends downward in time with a maximum value near the surface in October. The lagged correlation becomes insignificant in November, indicating that the surface responses to the stratospheric ozone variability are reinforced within

just one lagged month.

**Table 1.2.** Cross-correlation coefficient between the monthly-mean 10-hPa ozone and 700-hPa PCI and the SAM index for the period of 2004–2018. The values that are statistically significant at the 95% confidence level are denoted with an asterisk.

| $O_3$ | AUG | | SEP | | OCT | | NOV | | DEC | |
|---|---|---|---|---|---|---|---|---|---|---|
| | PCI | SAM | PCI | SAM | PCI | SAM | PCI | SAM | PCI | SAM |
| AUG | -0.63* | 0.55* | -0.51 | 0.46 | 0.50 | -0.29 | -0.03 | -0.04 | 0.38 | -0.33 |
| SEP | -0.15 | 0.04 | -0.03 | -0.11 | **0.67*** | **-0.68*** | 0.44 | -0.46 | 0.16 | -0.17 |
| OCT | 0.23 | -0.26 | 0.33 | -0.30 | 0.20 | -0.33 | **0.56*** | **-0.55*** | 0.15 | -0.13 |
| NOV | 0.31 | -0.26 | 0.33 | -0.38 | 0.30 | -0.39 | 0.33 | -0.35 | -0.03 | 0.05 |
| DEC | 0.08 | -0.04 | 0.58* | -0.53* | 0.12 | -0.23 | 0.35 | -0.22 | 0.04 | 0.11 |

Table 1.2 confirms the finding of Figure 3.2c. The cross-correlation coefficients between the polar-cap-averaged ozone at 10 hPa and 700-hPa PCI and those between the ozone and SAM index are summarized. Statistically significant values are observed between September ozone, and the one-month lagged tropospheric indices with correlation coefficients of 0.67 for PCI and -0.68 for SAM index. Note that SAM represents a seesaw-like mass change between mid- and high-latitudes, and its positive phase corresponds to the anomalous low pressure in the high latitudes. Therefore, SAM index is negatively correlated with PCI. The downward correlations are also present between October ozone and November tropospheric indices. However, they are weaker than the correlation coefficients in September.

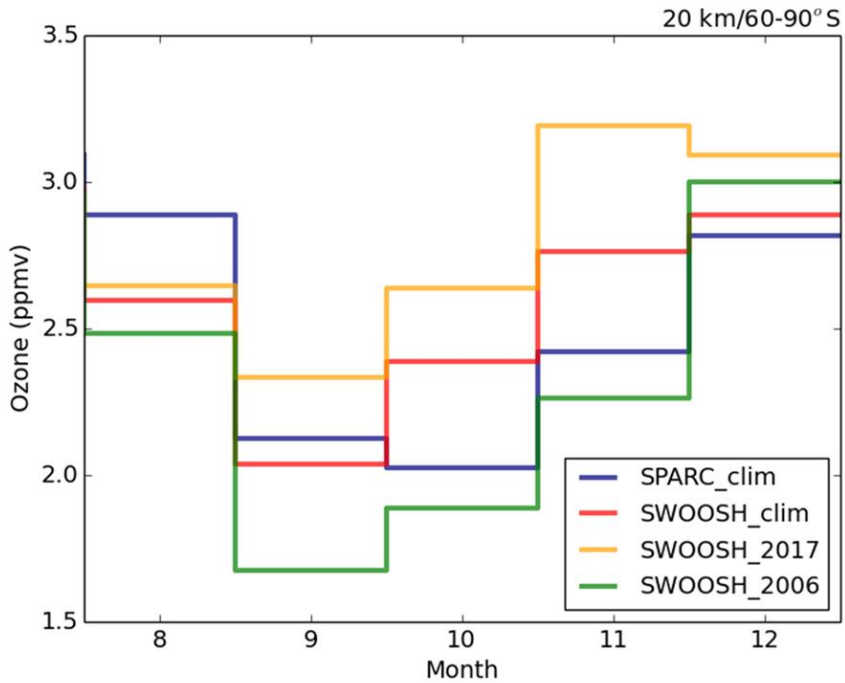


**Figure 3.3.** Model external forcing versus observation ozone averaged for south 60°S at 20 km as a function of the month (August to December).

### 3.3.2. Stratosphere-troposphere downward coupling

The Antarctic springtime ozone anomaly is significantly linked to the tropospheric circulation anomaly on interannual timescale (Son et al. 2013). Figure 3.4 shows their connection in the last three decades. It depicts the time pressure evaluation of lagged correlation coefficients between September mean TCO and daily PCI of ERA5 at all levels as a function of calendar day for the period of 1991–2020. The detrended data are used. To focus on S2S timescale, ERA5 PCI is smoothed by applying a 14-day moving average. Here, we use ERA5 TCO instead of SWOOSH ozone in order to extend the analysis period. The ERA5 TCO is derived from the modified version of the ozone parameterization of Cariolle and Deque (1986) as delineated by Cariolle and Teyssedre (2007). Various satellite observations over different time periods, such as MIPAS, MLS, OMI, GOME, GOME-2, and SBUV, are assimilated with variational bias corrections (Hersbach et al. 2019, 2020). Although TCO represents the ozone in a column of air extending from the surface to the top of the atmosphere, it is dominated by ozone within the stratosphere.

Figure 3.4a shows that September TCO is positively correlated with September PCI in the stratosphere. This relationship can be explained by the stratospheric circulation as introduced earlier. A positive PCI (or negative SAM index) is typically associated with a weak polar vortex which results from the upward

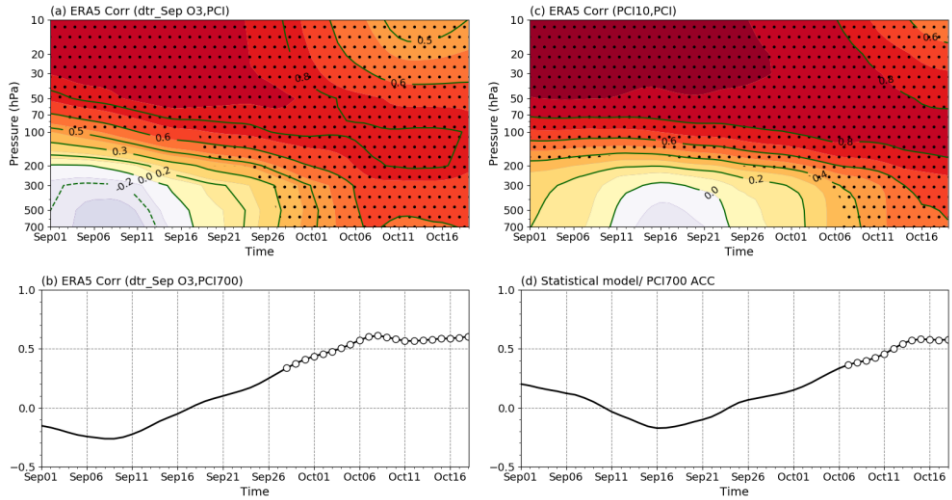


**Figure 3.4.** (a) Time-pressure distribution of lagged correlation coefficient between detrended September total column ozone anomaly and 14-day running averaged PCI during the period of 1991–2020. Statistically significant values are hatched at the 95% confidence level. (b) Same as (a) but for the PCI at 700 hPa. Open circles denote the values which are statistically significant at the 95% confidence level. (c), (d) Same as (a), (b) but for PCI predicted by a linear regression model based on 10-hPa PCI on 1st September.

wave propagation from the troposphere. The associated meridional circulation transports ozone from low latitudes to the pole, increasing polar stratospheric ozone.

Unlike in the stratosphere, a negative correlation appears in the troposphere in early to mid-September (Fig. 3.4a). Although not statistically significant, this vertical dipole, i.e., a positive correlation in the stratosphere and a negative correlation in the troposphere, could be partly explained by ozone radiative forcing in the stratosphere. Jucker and Goyal (2022) argued that the enhanced static stability at the mid- to high-latitudes in the lower stratosphere due to ozone shortwave heating could drive an equatorward wave deflection at the tropopause level. The resultant wave divergence in mid- to high latitudes then could lead to a thermally indirect circulation in the troposphere through the downward control (Haynes et al. 1991) and cause adiabatic cooling in the subpolar region. The net result is negative PCI at the high latitudes in the troposphere (see Fig. 4 of Jucker and Goyal, 2022).

The vertical dipole structure, which was referred to as “fast response” in Jucker and Goyal (2022), disappears in late September. A statistically significant positive correlation then emerges in the troposphere from weeks 5 to 8 (29th of September to 19th of October; Fig. 3.4 a, b) while a positive correlation is maintained in the stratosphere (Fig. 3.4a). This skill re-emergence results from the downward coupling. It is evident from Fig. 3.4a that a positive correlation propagates downward

in time from the upper stratosphere to the tropopause and becomes connected to the troposphere. Such a time-lagged downward connection, which was referred to as "slow response" in Jucker and Goyal (2022), represents a canonical stratosphere-troposphere dynamical coupling (e.g., Seviour et al., 2014; Saggioro and Shepherd, 2019).

Seviour et al. (2014) showed that a simple regression model utilizing the polar vortex variability can explain this skill re-emergence (see Fig. 7b of Seviour et al. 2014). When the similar regression model, based on 10-hPa PCI on 1st September, is applied to ERA5 data, the downward coupling is well captured at weeks 6 to 7 (Fig. 3.4 c, d). However, compared to Fig. 3.4 a-b, the vertical dipole in early and mid-September is weak and the time of skill re-emergence is delayed to mid-October. This result may indicate that the ozone radiative forcing leads to a stronger fast response and an earlier slow response.

It is worth to note that the SAM index exhibits the longest timescale in November (Baldwin et al. 2003; Gerber et al. 2012). This November peak has typically been explained by the stratospheric variability and its downward coupling. However, the downward coupling shown in Fig. 3.4 starts to appear in October. This result is consistent with Lim et al. (2019) who showed that the stratosphere-troposphere coupling in the SH is strongest in October (see their Fig. 1b, c). Lim et

al. (2019) suggested that the timing of the downward coupling is determined by the polar vortex weakening. When the polar vortex substantially weakens earlier than normal during spring, the resultant wind anomaly tends to propagate downward to the surface in October and November although the mechanism of downward propagation still remains to be determined.

### 3.3.3. Tropospheric prediction skill by ozone forcing

The downward coupling shown in Fig. 3.4 is well captured by the reforecast experiments. Figure 3.5a shows the ACCs of PCI in the COZ experiment. High ACCs, which are statistically significant at the 95% confidence level, are maintained at all lead times in the stratosphere, indicating persistent stratospheric anomalies. However, the ACCs in the troposphere rapidly decrease after week 3. This result is consistent with Son et al. (2020) who reported that the stratospheric prediction skill is much higher than the tropospheric skill in austral spring.

In the troposphere, a significant prediction skill reappears later in COZ experiment (i.e., 6 weeks after model initialization). This skill re-emergence in mid-October is not sensitive to the ensemble size and the choice of the variable. The same result is obtained when only half ensemble members are randomly selected. Although not shown, similar results are robustly found in other S2S prediction models which differ in the horizontal and vertical resolutions, ensemble size, and reforecast period (see also Seviour et al. 2014; Byrne et al. 2019). Here, we note that week 6 is not necessarily the optimal lead time of the tropospheric skill re-emergence. It could slightly change for 1 week when the initialization date is varied. For instance, the skill re-emergence appears in late September in the S2S prediction models initialized in late August or early September (Figure 3.6).

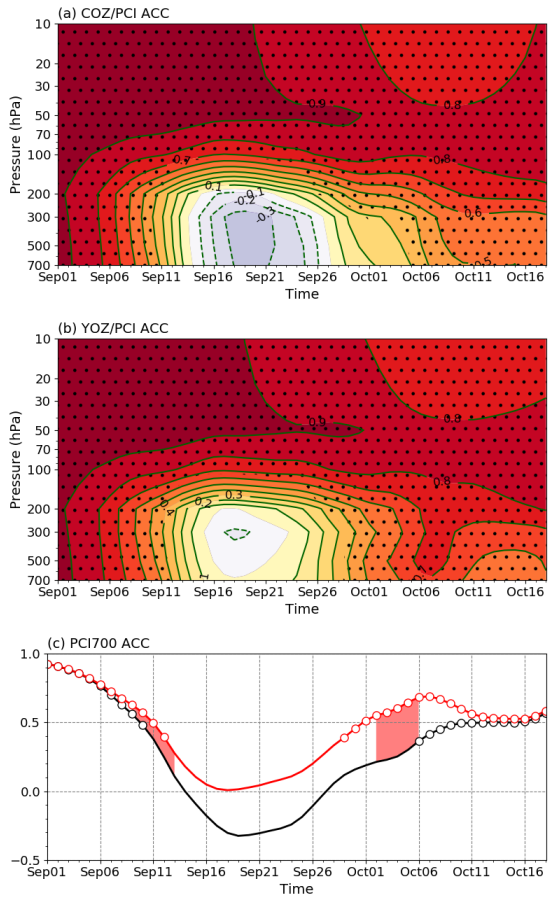


**Figure 3.5.** Anomaly correlation coefficients (ACCs) of 14-day running averaged PCI as a function of forecast lead time in (a) COZ and (b) YOZ experiments for the period of 2004–2020. The values which are statistically significant at the 95% confidence level are dotted. (c) ACCs of 700-hPa PCI in COZ experiment in black and those in YOZ experiment in red. Open circles denote the values which are statistically significant at the 95% confidence level. The forecast time when the ACC difference (YOZ minus COZ) is statistically significant at the 95% confidence level is shaded in pink. Note that October 6 in x-axis refers to the ACC at the forecast week 6–7.

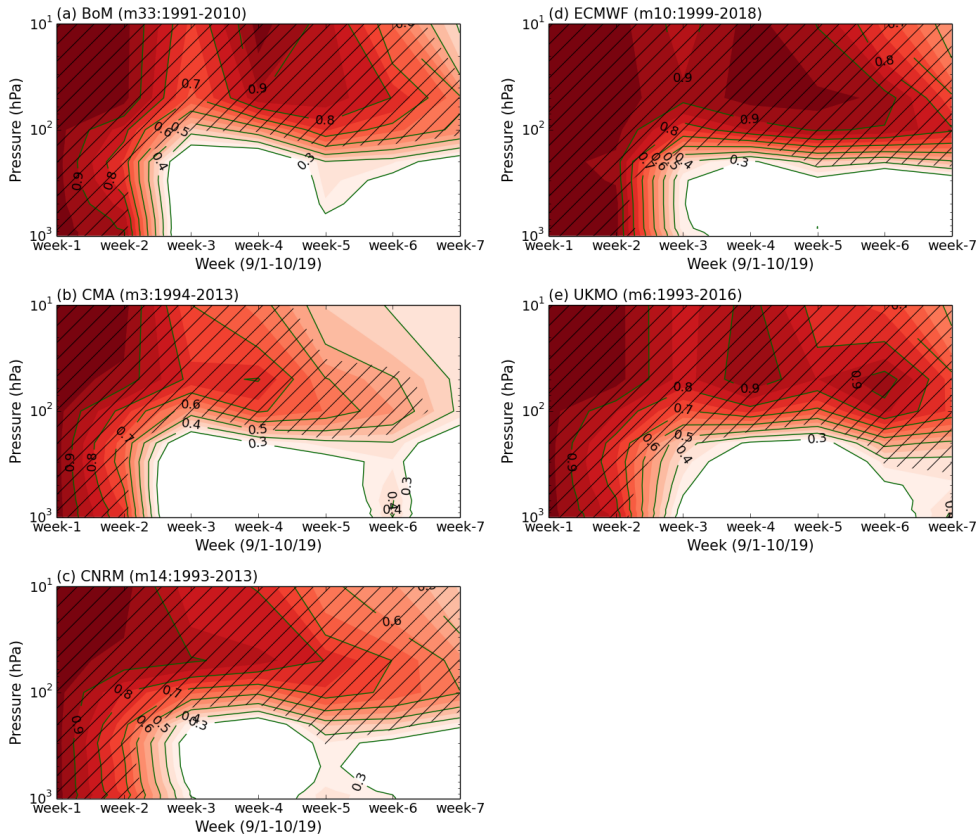


**Figure 3.6.** Same as of Fig. 3.4a but for four models archived for the S2S prediction. (a) Bureau of Meteorology, (b) China Meteorological Administration (CMA), (c) Centre National de Recherches Météorologiques (CNRM) of Météo-France, (d) European Centre for Medium-Range Weather Forecasts (ECMWF) and (e) United Kingdom Met Office (UKMO). The reforecast period is denoted at the top of each panel.

Although Fig. 3.5a clearly shows a downward influence in prediction skill, it does not delineate the role of ozone radiative forcing. To quantify the ozone impact on S2S prediction, we compare the COZ experiment to the YOZ experiment. Figure 3.5b shows the ACCs of the YOZ experiment. As described in the Method section, this experiment is identical to the COZ experiment except in how stratospheric ozone is specified; that is, the only difference is that stratospheric ozone is prescribed with year-to-year varying observation. The overall prediction skill does not change much in the first few weeks. However, a notable difference appears in late September and October when the downward influence is pronounced in the COZ experiment (Fig. 3.5a). Most importantly, the tropospheric prediction skill of the YOZ experiment is higher than that of the COZ experiment during the whole forecast lead time (Fig. 3.5c). The ACC difference between YOZ and COZ experiments which is statistically significant at the 95% confidence level appears at week 1–2 and week 6–7 (pink shading). It is noteworthy from Fig. 3.5a that the lowest prediction skill in the troposphere is found in mid- to late September when the vertical dipole disappears or when the fast response is switched into the slow response (Fig. 3.4a). Although statistically insignificant, the lowest prediction skill is also improved in the YOZ experiment presumably due to a more realistic ozone downward coupling.

This result indicates that a more realistic ozone helps to improve

tropospheric prediction in October. Lim et al. (2018) indicated that the stratosphere-troposphere coupling mode in the SH is highly correlated with ozone concentration in spring and could affect the tropospheric predictability in October. By integrating a model similar to the one used in this study, Hendon et al. (2020) showed that SH circulation in October is better captured when a realistic ozone is prescribed in the model during the 2002 stratospheric sudden warming event. In this regard, our result confirms the finding of Lim et al. (2018) and generalizes the case study of Hendon et al. (2020).

The skill difference between COZ and YOZ experiments at week 6–7 is further quantified in Fig. 3.7 a and b for 700-hPa PCI. The root-mean-squared error (RMSE) is significantly reduced from COZ to YOZ experiments, while the ACC is significantly increased. The ACC difference and its sensitivity to the ensemble size or number of validation years are further tested in Fig. 3.7 c, d by conducting a nonparametric bootstrap resampling method. The sensitivity to the ensemble size (M) is first tested by randomly selecting M ensemble members when computing the ensemble mean prediction. This resampling is conducted 1,000 times, allowing multiple counts. Their average is then considered as a skill score for a given ensemble size M. It turns out that the YOZ experiment shows a higher ACC than the COZ experiment for all cases from M = 1 to M = 18 (Fig. 3.7c). Its difference from the COZ experiment becomes statistically significant if the ensemble size is equal to

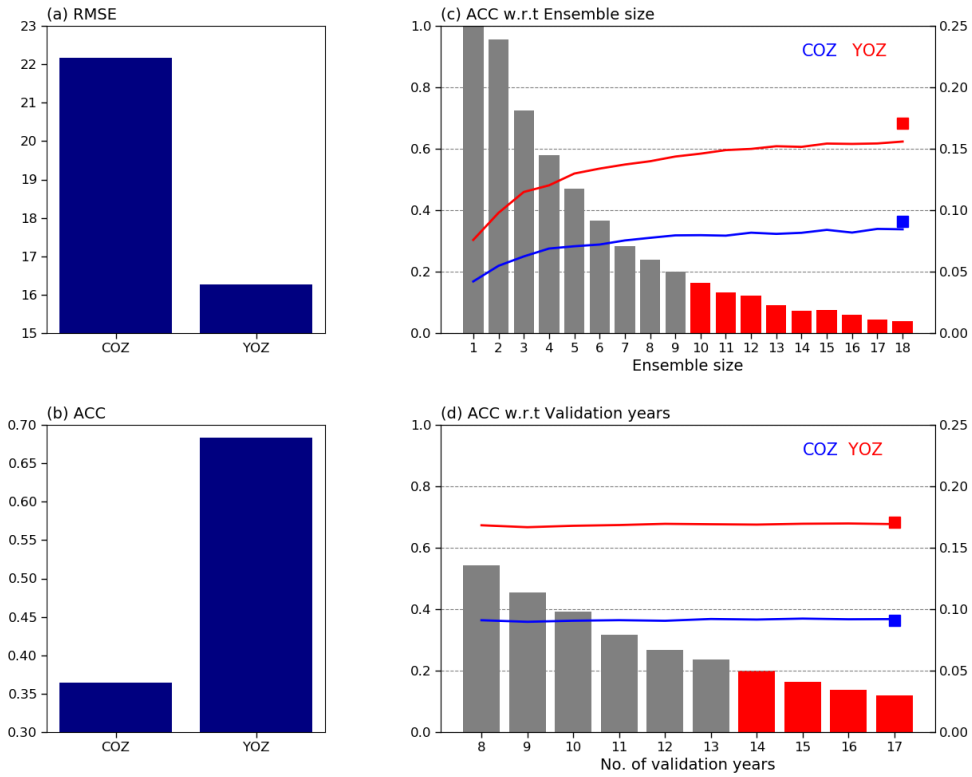


**Figure 3.7.** (a) Root-mean-squared error (RMSE) (m) and (b) ACC of 700-hPa PCI at the forecast week 6–7 in COZ and YOZ experiments. (c), (d) ACCs of week 6–7 PCI700 as a function of ensemble size and number of validation years. Each line indicates the average value of bootstrap-generated 1,000 ACCs. Square indicates the practical ACC shown in (b). Bars represent *p*-values for the ACC difference (YOZ minus COZ). The ACC difference is statistically significant at the 95% confidence level when the *p*-value is less than 0.05, which is denoted by red color.

or greater than 10. Note from Fig. 3.7c that the ACC difference for M = 18 is slightly smaller than the practical ACC difference (compare lines and squares) because a bootstrapping allows multiple counts.

A similar test is also conducted for a number of validation years. The number of validation years, N, is randomly selected. This process is also repeated 1,000 times and their average is considered as a skill score for a given number of validation years. Figure 3.7d shows that the YOZ-COZ skill difference is robust for N = 8 to N = 17. It becomes statistically significant when the number of validation years is equal to or greater than 14. These results suggest that the ACC difference between COZ and YOZ experiments shown in Fig. 3.5c is robust and not caused by chance.

An improved prediction skill in YOZ experiment is also evident at the surface for the regions that exhibit a strong impact of polar vortex variability (e.g., Lim et al.2019). Figure 3.8 illustrates the spatial distribution of RMSEs and ACCs at week 6–7 for maximum surface air temperature over Australia. Due to SAM-related surface climate variability, a reliable prediction skill appears in some regions in the COZ experiment (Fig. 3.8a), consistent with the SAM-related surface air temperature variability (e.g., Hendon et al. 2007). The prediction skill is enhanced in most regions when the year-to-year varying ozone is prescribed (Fig. 3.8b). A large

error reduction is especially found in eastern and southern Australia, while skill improvement is negligible in western and northern Australia.

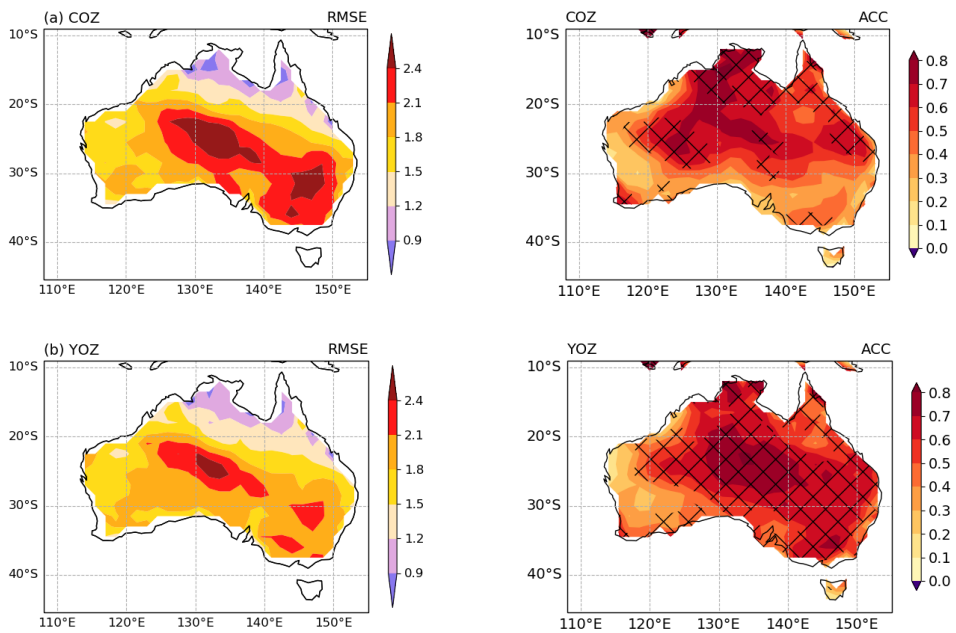


**Figure 3.8.** RMSE and ACC of week 6–7 maximum surface air temperature (T2Max) in (a) COZ and (b) YOZ experiments. In the right column, the values which are statistically significant at the 95% confidence level are dotted.

## 4. Summary and discussion

The cause of the TTL warm bias commonly found in various versions of the MetUM and many CMIP5 models is examined in this study, focusing on the potential role of the prescribed ozone in the model. The SPARC ozone data, which is used for most CMIP5 models, presents up to 50% higher ozone concentrations in the TTL than in the BDBP and up to 70% higher concentrations compared to the ozonesonde observations from the SHADOZ project. The standard AMIP simulation conducted using the MetUM with the prescribed SPARC ozone shows a significant warm bias in the TTL and a cold bias in the tropical middle-to-lower stratosphere. This bias pattern is reduced significantly by replacing the ozone data in the TTL and the tropical troposphere with the SHADOZ or BDBP ozone. Further sensitivity tests reveal that the improvement is made mostly by reducing the ozone concentration in the TTL within the 14–20 km layer. This result suggests that an uncertainty in the ozone amount in the TTL could lead to significant TTL temperature biases.

It should also be noted that the SHADOZ ozone and BDBP ozone show non-negligible differences in the TTL and lower stratosphere, particularly in the subtropical regions (Figure 1.2b). Although the BDBP database uses the SHADOZ ozone data for their ozone estimation, uncertainty can arise from merging the procedures of multiple datasets. In addition, the direct comparison between the

SPARC and SHADOZ ozone data given in this study may not be a fair analysis because their spatial and temporal samplings differ. Also, the SPARC ozone is mainly produced to provide background forcing for climate models rather than to reproduce individual ozone events. However, given the impact of TTL ozone on atmospheric temperature, further improvements in background ozone data will be greatly beneficial for weather and climate simulations.

It is also worth noting that the standard MetUM simulation presents a strong wet bias in the TTL and lower stratosphere (Figure 4.1a) compared to the SWOOSH data, which provides reliable ozone and water vapour estimations in the stratosphere from multiple satellite measurements (Davis et al.2016). This wet bias could affect the temperature in the TTL through a radiative process. However, the local radiative effect of water vapour is weak cooling in the TTL (Thuburn and Craig, 2002; Birner and Charlesworth, 2017; Ming et al. 2017); thus, the wet bias cannot be the cause of the TTL warm bias. The wet bias in the lower stratosphere is instead likely caused by the warm bias in the TTL through a weaker freeze-drying process (Holton et al. 1995) near the cold point.

In the experiment with the SHADOZ ozone, the wet bias is reduced significantly (Figure 4.1b). The improvement in water vapour is centred immediately above the tropical tropopause, where water vapour is transported following the

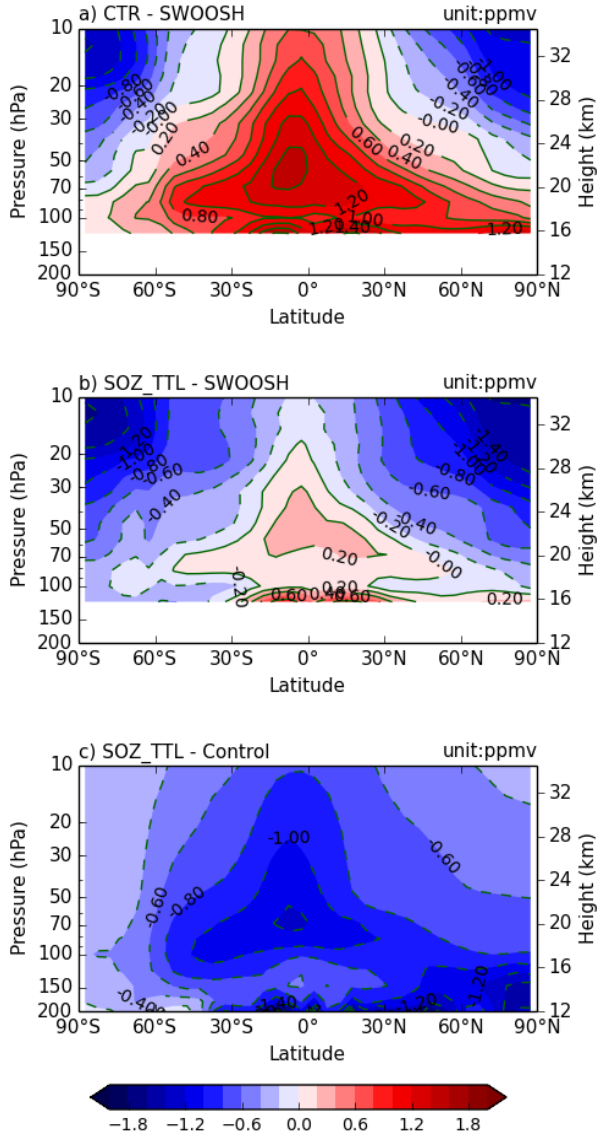


**Figure 4.1.** Latitude-pressure structure of specific humidity biases from (a) CTR and (b) SOZ_TTL runs against SWOOSH. (c) Specific humidity difference between SOZ_TTL and CTR runs (SOZ_TTL – CTR). Contour interval is 0.2 ppmv.

upward branch of the Brewer-Dobson circulation (BDC). The maximum difference between CTL and SOZ is ~1.2 ppmv in the tropical lower stratosphere, which is consistent with the 2-K temperature change at the cold-point tropopause based on the Clausius–Clapeyron calculation (the temperature dependency of the saturation vapour mixing ratio over ice is ~0.6 ppmv/K at 190 K and 90 hPa; Wexler, 1977). A slightly weaker but similar decrease in stratospheric water vapour was also found with the BDBP ozone (not shown). This improvement in the stratospheric water vapour is very important in climate simulation as it significantly changes the global radiation budget (e.g., Solomon et al. 2010). An accurate estimation of ozone forcing is required for future climate simulations.

Other radiatively active gases can also affect the TTL temperature, albeit minimally. Hardiman et al. (2015) describe the potential impact of methane and nitrous oxide on the TTL temperature. In simulations with interactive chemistry, methane and nitrous oxide contributed to a reduction in the TTL warm bias by 0.32 and 0.46 K, respectively. Other greenhouse gases may also alter the thermal structure in the TTL if their concentrations are substantially large (e.g., Thuburn and Craig, 2002). However, under the current level of atmospheric composition, ozone is likely the primary driver and the cause of the TTL warm bias found in many climate models.

The MJO convection tends to be more active and the prediction skill of

MJO in EQBO compared to WQBO during the boreal winter. It has been reported that the prediction skill of MJO is also high. Static stability change in the UTLS is being discussed as one of the mechanisms to explain the QBO-MJO connection. However, comprehensive climate models use ozone climatology, which underestimates the static stability change in UTLS on QBO phases. Therefore, this study investigates the role of ozone in the QBO-MJO relationship. More specifically, the effect of ozone-radiative feedback on MJO in the troposphere was investigated by prescribing climatology ozone (COZ) and the target year ozone (YOZ) with GloSea5.

The temperature anomalies in the COZ and YOZ experiments underestimate compared to the observation. However, the temperature anomaly in the YOZ experiment was improved by about 17 % compared to the COZ experiment by 0.4-0.5 K in the UTLS after about 20 days of initialization. However, there were no significant differences in MJO convection, amplitude and phase between the two experiments. Consequently, it was found that thermal stratification by ozone-radiative feedback did not significantly affect the change of MJO convection for the 2006 winter case.

Although the temperature difference between COZ and YOZ in the UTLS region is clear in this study, the reason why the QBO-MJO correlation cannot be

explained is presumed to be as follows. First, the lower stratospheric temperature response to QBO is not well simulated. Previous studies (e.g., Hendon and Abhik, 2018; Klotzbach et al. 2019; Lee and Klingaman, 2018) showed that MJO development for QBO was very sensitive to the effect of temperature in the UTLS. Although the zonal wind was simulated similarly to the observation, the secondary circulation was not well represented and hence the lower stratospheric cold anomaly by EQBO was not simulated (Figure 3). It implies that there is a large error in the lower stratospheric process of the model used in this study.

It is also presumed that the MJO is not well simulated in the model. As shown in Figures 5 and 6, the convection was well organized and the intensity of convection was maintained over time during the forecast period in the case of observation, whereas the development of convection was weak in the model experiment. Previous studies in which MJO convection was simulated qualitatively—despite weaker than observation—in the model showed significant changes in MJO depending on the QBO phases. If the MJO convection develops more vertically and its intensity and propagation can be reproduced in the model, the QBO modulation on MJO can be better captured.

Another possibility is that the amplitude and height of ozone-induced UTLS regional temperature changes may not be large enough to affect actual MJO

convection. Although there was a marginal improvement in the ozone-induced static stability in the UTLS, the difference was not large enough to affect the MJO convection. This is consistent with the result that the temperature change caused by QBO below 0.5 K has an insignificant effect on MJO (Martin et al. 2021). Moreover, since this may be highly case-dependent, further analysis of several cases in which ozone-induced temperature anomalies are intensified is likely to be necessary for the future.

Finally, chemical composition(s) such as ozone in the UTLS region as well as other physical processes may have influenced the QBO-MJO connection.

The cloud-radiative feedback related to cirrus clouds with ozone-radiative feedback is highlighted (Sakaeda et al. 2020; Son et al. 2007; Sun et al. 2019). Since the increase in cirrus near the tropical tropopause in EQBO can be caused by stronger MJO convection, it is necessary to discuss the causal relationship associated with cloud change.

This study is limited to a single case study. For a more quantitative QBO-MJO relationship study in the future, studies with a larger number of ensemble sizes and various cases are needed. In particular, it is necessary to consider not only EQBO but also WQBO cases.

It has been suggested that S2S prediction could be improved if the stratospheric state is represented more realistically (Seviour et al. 2014; Domeisen et al. 2020; Hendon et al. 2007). However, not many modeling studies have explored the impact of stratospheric conditions on the SH S2S prediction. In particular, the possible impact of stratospheric ozone has been rarely reported in the literature. Hendon et al. (2020) recently showed that stratospheric ozone can affect the surface prediction skill for the 2002 stratospheric sudden warming event, the first major sudden warming event in the SH. However, their results remain to be generalized with long-term reforecasts.

To assess the impact of stratospheric ozone on the S2S prediction, we performed two sets of GloSea5 reforecasts in which the stratospheric ozone concentration is prescribed with the long-term climatology (COZ) or year-to-year varying observation (YOZ). While the skill difference between the two experiments is relatively minor in the stratosphere, it is significant in the troposphere. Most importantly, the YOZ experiment outperforms the COZ experiment at all forecast lead times in October. Such an improvement is also evident at the surface over Australia.

Our result confirms that the ozone radiative forcing plays a critical role in the S2S prediction in the austral spring, generalizing Hendon et al. (2020). This

finding suggests that more realistic ozone is critical not only for the long-term climate simulation (e.g., Haase et al. 2020; Ivanciu et al. 2021; Li et al. 2016) but also for the operational S2S prediction. This is particularly true in the austral spring when the ozone radiative forcing is important.

Here, it should be stated that the ozone radiative feedback is not fully included in this study. The stratospheric ozone anomalies are prescribed as an external forcing to explore their thermodynamical and dynamical effects. The interplay between ozone and circulation is not taken into account. To evaluate the role of interactive ozone in the S2S prediction, further studies are required.

What determines the timing of the downward coupling (e.g., October) is a question yet to be answered, although observational data and model simulations show about a month lag (e.g., Seviour et al. 2014; Shaw et al. 2011). The related physical process is presumably similar to the long-term tropospheric response to the ozone depletion (e.g., Son et al. 2018) which is not yet fully understood. Several mechanisms have been proposed, which include downward control, eddy-mean flow interaction related to planetary and synoptic scale waves, eddy-eddy interactions, or combination of them (e.g., Hitchcock and Haynes, 2016; Orr et al. 2012; Yang et al. 2015; Martineau and Son, 2015). This topic needs more comprehensive analyses beyond ozone sensitivity tests.

# References


Abalos, M., W. Randel, D. Kinnison, and E. Serrano, 2013: Quantifying tracer transport in the tropical lower stratosphere using WACCM. *Atmospheric Chemistry and Physics*, **13**, 10591–10607. https://doi.org/10.5194/acp13-10591-2013

Abhik, S., and H. Hendon, 2019: Influence of the QBO on the MJO during coupled model multiweek forecasts. *Geophysical Research Letter*, **46**, 9213–9221. https://doi.org/10.1029/2019GL 083152

Andrews, D., J. Holton, and C. Leovy, 1987: Middle Atmosphere Dynamics, 489 pp., Academic Press, San Diego.

Back, S.-Y., J.-Y. Han, and S.-W. Son, 2020: Modeling evidence of QBO-MJO connection: A case study. *Geophysical Research Letter*, **47**, e2020GL089480. http://doi.org/10.1029/2020GL089480

Baldwin, M., L. Gray, T. Dunkerton, K. Hamilton, P. Haynes, W. Randel, J. Holton, M. Alexander, I. Hirota, T. Horinouchi, D. Jones, J. Kinnersley, C. Marquardt, K. Sato and M. Takahashi, 2001: The quasi-biennial oscillation. *Reviews of Geophysics*, **39**(2), 179–229. https://doi.org/10.1029/19999RG000073

Baldwin, M. and T. Dunkerton, 2001: Stratospheric Harbingers of Anomalous Weather Regimes. *Science*, **294**, 581–584. https://doi.org/10.1126/science.1063315

Baldwin, M., D. Stephenson, D. Thompson, T. Dunkerton, A. Charlton, A. O'Neill, 2003: Stratospheric memory and skill of extended-range weather forecasts. *Science*, **301**, 636–640. https://doi.org/10.1126/science.1087143

Baldwin, M., and D. Thompson, 2009: A critical comparison of stratosphere-troposphere coupling indices. *Quarterly Journal of the Royal Meteorological Society*, **135**, 1661–1672. https://doi.org/10.1002/qj.479

Birner, T. and E. Charlesworth, 2017: On the relative importance of radiative and dynamical heating for tropical tropopause temperatures. *Journal of Geophysical Research*, **122**, 6782–6797. https://doi.org/10.1002/2016JD026445

Blockley, E., M. Martin, A. McLaren, A. Ryan, J. Waters, D. Lea, I. Mirouze, K. Peterson, A. Sellar, D. Storkey, 2014: Recent development of the Met Office operational ocean forecasting system: an overview and assessment of the new Global FOAM forecasts. *Geoscientific Model Development*, **7**, 2613–2638. https://doi.org/10.5194/gmd-7-2613-2014

Bodeker, G., B. Hassler, P. Young, and R. Portmann, 2013: A vertically resolved, global, gap-free ozone database for assessing or constraining global climate model simulations. *Earth System Science Data*, **5**, 31–43. https://doi.org/10.5194/essd-5-31-2013

Bosilovich, M., S. Akella, L. Coy, R. Cullather, C. Draper, R. Gelaro, R. Kovach, Q. Liu, A. Molod, P. Norris, K. Wargan, W. Chao, R. Reichle, L. Takacs, Y. Vikhliaev, S. Bloom, A. Collow, S. Firth, G. Labow, G. Partyka, S. Pawson, O. Reale, S. Schubert, and M. Suarez, 2015: MERRA-2: Initial evaluation

of the climate. *NASA Technical Report Series on Global Modeling and Data Assimilation*. NASA/TM–2015-104606, **43**.

Brewer, A. 1949: Evidence for a world circulation provided by the measurements of helium and water vapour distribution in the stratosphere. *Quarterly Journal of the Royal Meteorological Society*, **75**, 351–363. https://doi.org/10.1002/qj.49707532603

Bushell, A., D. Jackson, N. Butchart, S. Hardiman, T. Hinton, S. Osprey, L. Gray, 2010: Sensitivity of GCM tropical middle atmospheric variability and climate to ozone and parameterized gravity wave changes. *Journal of Geophysical Research: Atmospheres*, **115**, D15101. https://doi.org/10.1029/2009JD013340

Butchart, N., A. Scaife, J. Austin, S. Hare, and J. Knight, 2003: Quasi-Biennial Oscillation in ozone in a coupled chemistry-climate model. *Journal of Geophysical Research: Atmospheres*, **108**, 4486. https://doi.org/10.1029/20–02JD003004

Butchart, N., J. Anstey, K. Hamilton, S. Osprey, C. McLandress, A. Bushell, Y. Kawatani, Y.-H. Kim, F. Lott, J. Scinocca, T. Stockdale, M. Andrews, O. Bellprat, P. Braesicke, C. Cagnazzo, C.-C. Chen, H.-Y. Chun, M. Dobrynin, R. Garcia, J. Garcia-Serrano, L. Gray, L. Holt, T. Kerzenmacher, H. Naoe, H. Pphlmann, J. Richer, A. Scaife, V. Schenzinger, F. Serva, S. Versick, S. Watanabe, K. Yoshida, and S. Yukimoto, 2018: Overview of experiment design and comparison of models participating in phase 1 of the SPARC quasi-biennial oscillation initiative (QBOi). *Geoscientific Model Development*, **11**(3), 1009–1032. https://doi.org/10.5194/gmd-2017-187

Byrne, N., and T. Shepherd, 2018: Seasonal persistence of circulation anomalies in the Southern Hemisphere stratosphere and its implications for the troposphere. *Journal of Climate*, **31**, 3467–3483. https://doi.org/10.1175/JC–LI-D-17-0557.1

Byrne, N., T. Shepherd, and I. Polichtchouk, 2019: Subseasonal-to-seasonal predictability of the Southern Hemisphere eddy-driven jet during austral spring and early summer. *Journal of Geophysical Research*: *Atmospheres*, **124**, 6841–6855. https://doi.org/10.1029/2018JD030173

Cariolle, D., and M. Deque, 1986: Southern hemisphere medium-scale waves and total ozone disturbances in a spectral general circulation model. *Journal of Geophysical Research*: *Atmospheres*, **91**, 10825–10846. https://doi.org/10.1–029/JD091iD10p10825

Cariolle, D., and H. Teyssedre, 2007: A revised linear ozone photochemistry parameterization for use in transport and general circulation models: multi-annual simulations. *Atmospheric Chemistry and Physics*, **7**, 2183–2196. https://doi.org/10.5194/acp-7-2183-2007

Chae, J.-H. and S. Sherwood, 2007: Annual temperature cycle of the tropical tropopause: a simple model study. *Journal of Geophysical Research*: *Atmospheres*, **112**, D19111. http://doi.org/10.1029/2006JD007956

Charlton-Perez, A., M. Baldwin, T. Birner, R. Black, A. Butler, N. Calvo, N. Davis, E. Gerber, N. Gillett, S. Hardiman, J. Kim, K. Krüger, Y.-Y. Lee, E. Manzini, B. McDaniel, L. Polvani, T. Reichler, T. Shaw, M. Sigmond, S.-W. Son, M. Toohey, L. Wilcox, S. Yoden, B. Christiansen, F. Lott, D. Shindell, S. Yukimoto, and S. Watanabe, 2013: On the lack of stratospheric dynamical

variability in low-top versions of the CMIP5 models. *Journal of Geophysical Research: Atmospheres*, **118**, 2494–2505. https://doi.org/10.10–02/jgrd.50125

Choi, J., and S.-W. Son, 2019: Stratospheric initial condition for skillful surface prediction in the ECMWF model. *Geophysical Research Letters*, **21**, 12556–12564. https://doi.org/10.1029/2019GL083519

Cionni, I., V. Eyring, J. Lamarque, W. Randel, D. Stevenson, F. Wu, G. Bodeker, T. Shepherd, D. Shindell, and D. Waugh, 2011: Ozone database in support of CMIP5 simulations: results and corresponding radiative forcing. *Atmospheric Chemistry and Physics*, **11**(21), 11267–11292. https://doi.org/–10.5194/acp-11-11267-2011

Collimore, C., D. Martin, M. Hitchman, A. Huesmann, and D. Waliser, 2003: On the relationship between the QBO and tropical deep convection. *Journal of Climate*, **16**(15), 2552–2568. https://doi.org/10.1175/1520-0442(2003)016%–3C2552:OTRBTQ%3E2.0. CO;2

Copernicus Climate Change Service, 2017: ERA5: Fifth Generation of ECMWF Atmospheric Reanalyses of the Global Climate. Copernicus Climate Change Service Climate Data Store (CDS). ECMWF. Available at: https://cds.clima–te.copernicus.eu/cdsapp#!/home

Cordero, E., and P. Forster, 2006: Stratospheric variability and trends in models used for the IPCC AR4. *Atmospheric Chemistry and Physics*, **6**, 5369–5380. https://doi.org/10.5194/acp-6-5369-2006

Cusack, S., J. Edwards, and J. Crowther, 1999: Investigating k distribution methods for parameterizing gaseous absorption in the Hadley Centre Climate Model.

*Journal of Geophysical Research: Atmospheres*, **104**, 2051–2057. https://doi.–org/10.1029/1998JD200063

Davis, S., K. Rosenlof, B. Hassler, D. Hurst, W. Read, H. Vömel, H. Selkirk, M. Fujiwara, and R. Damadeo, 2016: The Stratospheric Water and Ozone Satellite Homogenized (SWOOSH) database: a long-term database for climate studies. *Earth System Science Data*, **8**, 461–490. https://doi.org/10.5194/essd-8-461-2016

Dee, D., S. Uppala, A. Simmons, P. Berrisford, P. Poli, S. Kobayashi, U. Andrae, M. Balmaseda, G. Balsamo, P. Bauer, P. Bechtold, A. Beljaars, L. van de Berg, J. Bidlot, N. Bormann, C. Delsol, R. Dragani, M. Fuentes, A. Geer, L. Haimberger, S. Healy, H. Hersbach, E. Hólm, L. Isaksen, P. Kållberg, M. Köhler, M. Matricardi, A. McNally, B. Monge-Sanz, J. Morcrette, B.-K. Park, C. Peubey, P. de Rosnay, C. Tavolato, J. Thépaut, and F. Vitart, 2011: The ERA-interim reanalysis: configuration and performance of the data assimilation system. *Quarterly Journal of the Royal Meteorological Society*, **137**, 553–597. https://doi.org/10. 1002/qj.828

Dobson, G. 1956: Origin and distribution of the polyatomic molecules in the atmosphere. *Proceedings of the Royal Society A: Mathematical, Physical and Engineering Sciences*, **236**, 187–193. https://doi.org/10.1098/rspa.1956.–0127

Domeisen, D., A. Butler, A. Charlton-Perez, B. Ayarzaguena, M. Baldwin, E. Dunn-Sigouin, J. Furtado, C. Garfinkel, P. Hitchcock, A. Karpechko, H. Kim, J. Knight, A. Lang, E.-P. Lim, A. Marshall, G. Roff, C. Schwartz, I. Simpson, S.-W. Son, M. Taguchi, 2019: The role of the stratosphere in subseasonal to seasonal prediction Part I: Predictability of the stratosphere. *Journal of*

*Geophysical Research: Atmospheres*, **125**, e2019JD030920. https://doi.org/10.1029/2019JD030920

Edwards, J., and A. Slingo, 1996: Studies with a flexible new radiation code. I: Choosing. *Quarterly Journal of the Royal Meteorological Society*, **122**, 689–719. https://doi.org/10.1002/qj.49712253107

Folkins, I. and R. Martin, 2005: The vertical structure of tropical convection and its impact on the budgets of water vapor and ozone. *Journal of the Atmospheric Sciences*, **62**, 1560–1573. https://doi.org/10.1175/JAS3407.1

Fortuin, J., and H. Kelder, 1998: An ozone climatology based on ozonesonde and satellite measurements. *Journal of Geophysical Research: Atmospheres*, **103**, 31709–31734. https://doi.org/10.1029/1998JD200008

Fueglistaler, S., A. Dessler, T. Dunkerton, I. Folkins, Q. Fu, and P. Mote, 2009: Tropical tropopause layer. *Reviews of Geophysics*, **47**, RG1004. https://doi.org/10.1029/2008RG000267

Fueglistaler, S., B. Legras, A. Beljaars, J.-J. Morcrette, A. Simmons, A. Tompkins, and S. Uppala, 2009: The diabatic heat budget of the upper troposphere and lower/mid stratosphere in ECMWF reanalyses. *Quarterly Journal of the Royal Meteorological Society*, **135**, 21–37. https://doi.org/10.1002/qj.361

Fueglistaler, S., P. Haynes, and P. Forster, 2011: The annual cycle in lower stratospheric temperatures revisited. *Atmospheric Chemistry and Physics*, **11**, 3701–3711. https://doi.org/10.5194/acp-11-3701-2011

Gerber, E., A. Butler, N. Calvo, A. Charlton-Perez, M. Giorgetta, E. Manzini, J. Perlwitz, L. Polvani, F. Sassi, A. Scaife, T. Shaw, S.-W. Son, S. Watanabe,

2012: Assessing and understanding the impact of stratospheric dynamics and variability on the earth system. *Bulletin of the American Meteorological Society*, **93**, 845–859. https://doi.org/10.1175/BAMS-D-11-00145.1

Gerber, E., and Son S.-W., 2014: Quantifying the summertime response of the austral jet stream and Hadley cell to stratospheric ozone and greenhouse gases. *Journal of Climate*, **27**, 5538–5559. https://doi.org/10.1175/JCLI-D-13-00539.1

Gettelman, A., P. Forster, M. Fujiwara, Q. Fu, H. Vömel, L. Gohar, C. Johanson, and M. Ammerman, 2004: Radiation balance of the tropical tropopause layer. *Journal of Geophysical Research: Atmospheres*, **109**, D07103. https://doi.org/10.1029/2003JD004190

Gettelman, A., M. Hegglin, S.-W. Son, J. Kim, M. Fujiwara, T. Birner, S. Kremser, M. Rex, J. Anel, H. Akiyoshi, J. Austin, S. Bekki, P. Braesike, C. Bruhl, N. Butchart, M. Chipperfield, M. Dameris, S. Dhomse, H. Garny, S. Hardiman, P. Jockel, D. Kinnison, J. Lamarque, E. Mancini, M. Marchand, M. Michou, O. Morgenstern, P. Pawson, G. Pitari, D. Plummer, J. Pyle, E. Rozanov, J. Scinocca, T. Shepherd, K. Shibata, D. Smale, H. Teyssedre, and W. Tian, 2010: Multimodel assessment of the upper troposphere and lower stratosphere: tropics and global trends. *Journal of Geophysical Research: Atmospheres*, **115**, D00M08. https://doi.org/10.1029/2009JD013638

Goddard, L., A. Kumar, A. Solomon, D. Smith, G. Boer, P. Gonzalez, V. Kharin, W. Merryfield, C. Deser, S. Mason, B. Kirtman, R. Msadek, R. Sutton, E. Hawkins, T. Fricker, G. Hegerl, C. Ferro, D. Stephenson, G. Meehl, T. Stockdale, R. Burgman, A. Greene, Y. Kushnir, M. Newman, J. Carton, I. Fukumori, and T. Delworth, 2013: A verification framework for interannual-

to-decadal predictions experiments. *Climate Dynamics*, **40**, 245–272. https://doi.org/10.1007/s00382-012-1481-2

Gong, D., and Wang, S., 1999: Definition of Antarctic Oscillation index. *Geophysical Research Letters*, **26**, 459–462. https://doi.org/10.1029/1999GL900003

Gray, L., J. Anstey, Y. Kawatani, H. Lu, S. Osprey, and V. Schenzinger, 2018: Surface impacts of the Quasi Biennial Oscillation. *Atmospheric Chemistry and Physics*, **18**(11), 8227. https://doi.org/10.5194/acp-18-8227-2018

Hardiman, S., I. Boutle, A. Bushell, N. Butchart, M. Cullen, P. Field, K. Furtado, J. Manners, S. Milton, C. Morcrette, F. O'Connor, B. Shipway, C. Smith, D. Walters, M. Willett, K. Williams, N. Wood, N. Abraham, J. Keeble, A. Maycock, J. Thuburn, and M. Woodhouse, 2015: Processes controlling tropical tropopause temperature and stratospheric water vapor in climate models. *Journal of Climate*, **28**, 6516–6535. https://doi. org/10.1175/JCLI-D-15-0075.1

Haase, S., J. Fricke, T. Kruschke, S. Wahl, K. Matthes, 2020: Sensitivity of the Southern Hemisphere circumpolar jet response to Antarctic ozone depletion: prescribed versus interactive chemistry. *Atmospheric Chemistry and Physics* **20**, 14043–14061. https://doi.org/10.5194/acp-20-14043-2020

Haynes, P., M. McIntyre, T. Shepherd, C. Marks, K. Shine, 1991: On the "Downward Control" of extratropical diabatic circulations by eddy-induced mean zonal forces. *Journal of the Atmospheric Sciences*, **48**(4):651–678. https://doi.org/10. 1175/1520-0469(1991)048%3c0651:otcoed%3e2.0.co;2

Hassler, B., G. Bodeker, and M. Dameris, 2008: Technical note: a new global database of trace gases and aerosols from multiple sources of high vertical resolution measurements. *Atmospheric Chemistry and Physics*, **8**, 5403–5421. https://doi.org/10.5194/acpd-8-7657-2008

Hendon, H., D. Thompson, and M. Wheeler, 2007: Australian rainfall and surface temperature variations associated with the Southern Hemisphere Annular Mode. *Journal of Climate*, **20**, 2452–2467. https://doi.org/10.1175/JCLI4134.1

Hendon, H., and S. Abhik, 2018: Differences in vertical structure of the Madden-Julian oscillation associated with the Quasi-Biennial Oscillation. *Geophysical Research Letters*, **45**, 4419–4428. https://doi.org/10.1029/2018GL077207

Hendon, H., E.-P. Lim and S. Abhik, 2020: Impact of interannual ozone variations on the downward coupling of the 2002 Southern Hemisphere stratospheric warming. *Journal of Geophysical Research: Atmospheres*, **125**, e2020JD032952. https://doi.org/10.1029/2020JD032952

Hersbach, H., and Dee, D. 2016: ERA5 reanalysis is in production. ECMWF Newsletter **147**, ECMWF, Reading, UK, Available from https://www.ecmwf.int/en/newsletter/147/news/era5-reanalysis-production

Hersbach, H., B. Bell, P. Berrisford, A. Horányi, J. Muños-Sabater, J. Nicolas, R. Radu, D. Schepers, A. Simmons, C. Soci, D. Dee, 2019: Global reanalysis: goodbye ERA-Interim, hello ERA5. ECMWF, https://doi.org/10.21957/vf291hehd7

Hersbach, H., B. Bell, P. Berrisford, S. Hirahara, A. Horányi, J. Muños-Sabater, J. Nicolas, C. Peubey, R. Radu, D. Schepers, A. Simmons, C. Soci, S. Abdalla, X. Abellan, G. Balsamo, P. Bechtold, G. Biavati, J. Bidlot, M. Bonavita, G. De Chiara, P. Dahlgren, D. Dee D, M. Diamantakis, R. Dragani, J. Flemming, R. Forbes, M. Fuentes, A. Geer, L. Haimberger, S. Healy, R. Hogan, E. Hólm, M. Janisková, S. Keeley, P. Laloyaux, P. Lopez, C. Lupu, G. Radnoti, P. de Rosnay, I. Rozum, F. Vamborg, S. Villaume, and J.-N. Thepaut, 2020: The ERA5 global reanalysis. *Quarterly Journal of the Royal Meteorological Society,* **146**, 1999–2049. https://doi.org/10.1002/qj.3803

Hio, Y., and S. Yoden, 2005: Interannual variations of the seasonal march in the Southern Hemisphere stratosphere for 1979–2002 and characterization of the unprecedented year 2002. *Journal of the Atmospheric Sciences*, **62**, 567–580. https://doi.org/10.1175/JAS-3333.1

Hitchcock, P., and Haynes, P. 2016: Stratospheric control of planetary waves. *Geophysical Research Letters*, **43**, 11884–11892. https://doi.org/10.1002/2016GL071372

Ho, M., A. Kiem, and Verdon-Kidd, D., 2012: The southern annual mode: a comparison of indices. *Hydrology and Earth Systerm Sciences*, **16**, 967-982. https://doi.org/10.5194/hess-16-967-2012

Holton, J., P. Haynes, M. McIntyre, A. Douglass, R. Rood, and L. Pfister, 1995: Stratosphere-troposphere exchange. *Reviews of Geophysics*, **33**(4), 403–439. https://doi.org/10.1029/95RG02097

Inness, A., F. Baier, A. Benedetti, I. Bouarar, S. Chabrillat, H. Clark, C. Clerbaux, P. Coheur, R. Engelen, Q. Errera, J. Flemming, M. George, C. Granier, J.

Hadji-Lazaro, V. Huijnen, D. Hurtmans, L. Jones, J. Kaiser, J. Kapsomenakis, K. Lefever, J. Leitão, M. Razinger, A. Richter, M. Schultz, A. Simmons, M. Suttie, O. Stein, J.-N. Thépaut1, V. Thouret, M. Vrekoussis, C. Zerefos, and the MACC team, 2013: The MACC reanalysis: an 8 yr data set of atmospheric composition. *Atmospheric Chemistry and Physics*, **13**, 4073-4109. https://doi.org/10.5194/acp-13-4073-2013

Ivanciu, I., K. Matthes, S. Wahl, J. Harlaß, and A. Biastoch, 2021: Effects of prescribed CMIP6 ozone on simulating the Southern Hemisphere atmospheric circulation response to ozone depletion. *Atmospheric Chemistry and Physics*, **21**, 5777–5806. https://doi.org/10.5194/acp-21-5777-2021

Janiga, M., C. Schreck, J. Ridout, M. Flatau, N. Barton, E. Metzger, and C. A. Reynolds, 2018: Subseasonal Forecasts of Convectively Coupled Equatorial Waves and the MJO: Activity and Predictive Skill, *Monthly Weather Review*, **146**, 2337–2360. https://doi.org/10.1175/MWR-D-17-0261.1

Jucker, M., and R. Goyal, 2022: Ozone-forced southern annular mode during Antarctic stratospheric warming events, *Geophysical Research Letters*, **49**, e2021GL095270. https://doi.org/10.1029/2021GL095270

Kang, S., L. Polvani, J. Fyfe, and M. Sigmond, 2011: Impact of polar ozone depletion on subtropical precipitation, *Science*, **332**, 951–955. https://doi.org/10.1126/science.1202131

Kim, D., E. Maloney, and C. Zhang, 2019: Review: MJO propagation over the Maritime Continent. In C.-P. Chang et al. (Eds.), The multiscale global monsoon system, **11**, World Scientific Series on Asia-Pacific Weather and

Climate. World Scientific, Singapore. https://doi.org/10.1142/9789811216602_0021

Kim, H., J. Richter, and Z. Martin, 2019: Insignificant QBO-MJO prediction skill relationship in the SubX and S2S subseasonal reforecasts. *Journal of Geophysical Research: Atmospheres*, **124**, 12655–12666. https://doi.org/10.1029/2019JD031416

Kim, J., and S.-W. Son, 2015: Formation and maintenance of the tropical cold-point tropopause in a dry dynamic-core GCM. *Journal of the Atmospheric Sciences*, **72**, 3097–3115. https://doi.org/10.1175/JAS-D-14-0338.1

Kim, J., K. Grise, and S.-W. Son, 2013: Thermal characteristics of the cold-point tropopause region in CMIP5 models. *Journal of Geophysical Research: Atmospheres*, **118**, 8827–8841. https://doi.org/10.1002/jgrd. 50649

Kim, H., P. Webster, V. Toma, and D. Kim, 2014: Predictability and prediction skill of the MJO in two operational forecasting systems. *Journal of Climate*, **27**(14), 5364–5378. https://doi.org/10.1175/JCLI-D-13-00480.1

Kim, H., 2017: The impact of the mean moisture bias on the key physics of MJO propagation in the ECMWF reforecast. *Journal of Geophysical Research: Atmospheres*, **122**, 7772–7784. https://doi.org/10.1002/2017JD027005

Kim, H., F. Vitart, and D. Waliser, 2018: Prediction of the Madden–Julian oscillation: A review. *Journal of Climate*, **31**, 9425–9443. https://doi.org/10.1175/JCLI-D-18-0210.1

Kim, H., J. Richter, and Z. Martin, 2019: Insignificant QBO-MJO prediction skill relationship in the SubX and S2S subseasonal reforecasts. *Journal of*

*Geophysical Research: Atmospheres*, **124**, 12655–12666. https://doi.org/10.1029/2019JD031416

Kim, H., J. Caron, J. Richter, and I. Simpson, 2020: The lack of QBO-MJO connection in CMIP6 models. *Geophysical Research Letters*, **47**, e2020GL087295. https://doi.org/10.1029/2020GL087295

Klotzbach, P., S. Abhik, H. Hendon, M. Bell, C. Lucas, A. Marshall, and E. Oliver, 2019: On the emerging relationship between the stratospheric Quasi-Biennial Oscillation and the Madden-Julian oscillation. *Scientific Reports*, **9**, 2981. https://doi.org/10.1038/s41598- 019-40034-6

Kolstad, E., and A. Charlton-Perez, 2010: Observed and simulated precursors of stratospheric polar vortex anomalies in the Northern Hemisphere. *Climate Dynamics*, **37**, 1443–1456. https://doi.org/10.1007/s00382-010-0919-7

Lamarque, J.-F., T. Bond, V. Eyring, C. Granier, A. Heil, Z. Klimont, D. Lee, C. Liousse, A. Mieville, B. Owen, M. Schultz, D. Shindell, S. Smith, E. Stehfest, J. Van Aardenne, O. Copper, M. Kainuma, N. Mahowald, J. McConnell, V. Naik, K. Riahi, and D. Van Vuuren, 2010: Historical (1850–2000) gridded anthropogenic and biomass burning emissions of reactive gases and aerosols: methodology and application. *Atmospheric Chemistry and Physics*, **10**, 7017–7039. https://doi.org/10.5194/acp-10-7017-2010

Lee, J., and N. Klingaman, 2018: The effect of the quasi-biennial oscillation on the Madden-Julian oscillation in the Met Office unified model global ocean mixed layer configuration. *Atmospheric Science Letters*, **19**(5), e816. https://doi.org/10.1002/asl.816

Liess, S., and M. Geller, 2012: On the relationship between QBO and distribution of tropical deep convection. *Journal of Geophysical Research: Atmospheres*, **117**, D03108. https://doi.org/10.1029/2011JD016317

Li, D., K. Shine, and L. Gray, 1995: The role of ozone-induced heating anomalies in the Quasi-Biennial Oscillation. *Quarterly Journal of the Royal Meteorological Society*, **121**(524), 937–943. https://doi.org/10.1002/qj.49712152411

Li, F., Y. Vikhliaev, P. Newman, S. Pawson, J. Perlwitz, D. Waugh, A. Douglass, 2016: Impacts of interactive stratospheric chemistry on antarctic and southern ocean climate change in the Goddard Earth Observing System, version 5 (GEOS-5). *Journal of Climate*, **29**, 3199–3218. https://doi.org/10.1175/ JCLI-D-15-0572.1

Liu, C., B. Tian, K.-F. Li, G. Manney, N. Livesey, Y. Yung, and D. Waliser, 2014: Northern Hemisphere mid-winter vortex- displacement and vortex-split stratospheric sudden warmings: Influence of the Madden-Julian oscillation and Quasi-Biennial Oscillation. *Journal of Geophysical Research: Atmospheres*, **119**, 12599–12620. https://doi.org/10.1002/2014JD021876

Lim, E.-P., H. Hendon, and D. Thompson, 2018: Seasonal evolution of stratosphere-troposphere coupling in the Southern Hemisphere and implications for the predictability of surface climate. *Journal of Geophysical Research: Atmospheres*, **123**, 12002-12016. https://doi.org/10.1029/2018JD029321

Lim, E.-P., H. Hendon, G. Boschat, D. Hudson, D. Thompson, A. Dowdy, J. Arblaster, 2019: Australian hot and dry extremes induced by weakenings of

the stratospheric polar vortex. *Nature Geoscience*, **12**(11), 896–901. https://doi.org/10.1038/s41561-019-0456-x

Lim, Y., S.-W. Son, and D. Kim, 2018: MJO prediction skill of the subseasonal-to-seasonal prediction models. *Journal of Climate*, **31**, 4075-4094. https://doi.org/10.1175/JCLI-D-17-0545.1

Lim, Y., S.-W. Son, A. Marshall, H. Hendon, and K.-H. Seo, 2019: Influence of the QBO on MJO prediction skill in the subseasonal-to-seasonal prediction models. *Climate Dynamics*, **53**(3-4), 1681–1695. https://doi.org/10.1007/s00382-019-04719-y

Lim, Y., and S.-W. Son, 2020: QBO-MJO connection in CMIP5 models. *Journal of Geophysical Research: Atmospheres*, **125**, e2019JD032157. https://doi.org/10.1029/2019JD032157

Lin, P., D. Paynter, Y. Ming, and V. Ramaswamy, 2016: Changes of the tropical tropopause layer under global warming. *Journal of Climate*, **30**, 1245–1258. https://doi.org/10.1175/JCLI-D-16-0457.1

MacLachlan C., A. Arribas, K. Peterson, A. Maidens, D. Fereday, A. Scaife, M. Gordon, M. Vellinga, A. Williams, R. Comer, J. Camp, and P. Xavier, 2015: Description of GloSea5: the Met Office high resolution seasonal forecast system. *Quarterly Journal of the Royal Meteorological Society*, **141**, 1072–1084. https://doi.org/10.1002/qj.2396

Madden, R., and P. Julian, 1971: Detection of a 40–50 day oscillation in the zonal wind in the tropical Pacific. *Journal of the Atmospheric Sciences*, **28**(5), 702–708. https://doi.org/10.1175/1520-0469(1971)028<0702:DOADOI>2.0.CO;2

Madden, R., and P. Julian, 1972: Description of Global-Scale Circulation Cells in the Tropics with a 40-50 Day Period. *Journal of the Atmospheric Sciences*, **29**, 1109–1123. https://doi.org/10.1175/1520-0469(1972)029<1109:DOGSCC>2.0.CO;2

Mariotti, A., P. Ruti, and M. Rixen, 2018: Progress in subseasonal to seasonal prediction through a joint weather and climate community effort. *Nature Partner Journals Climate and Atmospheric Science*, **1**, 4, https://doi.org/10.1038/s41612-018-0014-z

Martineau, P., and S.-W. Son, 2015: Onset of circulation anomalies during stratospheric vortex weakening events: the role of planetary-scale waves. *Journal of Climate*, **28**, 7347–7370. https://doi.org/10.1175/JCLI-D-14-00478.1

Marshall, A., H. Hendon, S.-W. Son, Y. Lim, 2017: Impact of the Quasi-Biennial Oscillation on predictability of the Madden-Julian oscillation. *Climate Dynamics*, **49**,1365–1377. https ://doi.org/10.1007/s0038 2-016-3392-0

Martin, Z., S. Wang, J. Nie, and A. Sobel, 2019: The impact of the QBO on MJO convection in cloud-resolving simulations. *Journal of the Atmospheric Sciences*, **76**, 669–688. https://doi.org/10.1175/JAS-D-18-0179.1

Martin, Z., F. Vitart, S. Wang, and A. Sobel, 2020: The impact of the stratosphere on the MJO in a forecast model. *Journal of Geophysics Research: Atmosphere*, **125**, e2019JD032106. https://doi.org/10.1029/2019jd032106

Martin, Z., C. Orbe, S. Wang, and A. Sobel, 2021: The MJO-QBO relationship in a GCM with stratospheric nudging. *Journal of Climate*, **34**, 4603–4624. https://doi.org/10.1175/JCLI-D-20-0636.1

Ming, A., A. Maycock, P. Hitchcock, and P. Haynes, 2017: The radiative role of ozone and water vapour in the annual temperature cycle in the tropical tropopause layer. *Atmospheric Chemistry and Physics*, **17**(9), 5677–5701. https://doi.org/10.5194/acp-17-5677-2017

Nie, J., and A. Sobel, 2015: Responses of tropical deep convection to the QBO: Cloud-resolving simulations. *Journal of the Atmospheric Sciences*, **72**(9), 3625–3638. https://doi.org/10.1175/JAS-D-15-0035.1

Nishimoto, E., and S. Yoden, 2017: Influence of the stratospheric quasi-biennial oscillation on the Madden–Julian oscillation during austral summer. *Journal of the Atmospheric Sciences*, **74**(4), 1105–1125. https://doi.org/10.1175/JAS-D-16-0205.1

Orr, A., T. Bracegirdle, J. Hosking, T. Jung, J. Haigh, T. Phillips, and W. Feng, 2012: Possible dynamical mechanisms for Southern Hemisphere climate change due to the ozone hole. *Journal of the Atmospheric Sciences*, **69**(10), 2917–2932. https://doi.org/10.1175/JASD-11-0210.1

Ploeger, F., P. Konopka, R. Müller, S. Fueglistaler, T. Schmidt, J. Manners, J.-U. Groo$\beta$, G. Günther, P. Forster, and M. Riese, 2012: Horizontal transport affecting trace gas seasonality in the Tropical Tropopause Layer (TTL). *Journal of Geophysical Research: Atmospheres*, **117**, D09303. https://doi.org/10.1029/2011JD017267

Pohlmann, H., W. Müller, M. Bittner, S. Hettrich, K. Modali, K. Pankatz, and J. Marotzke, 2019: Realisticquasi-biennial oscillation variability inhistorical and decadal hindcastsimulations using CMIP6 forcing. *Geophysical Research Letters*, **46**,14118–14125. https://doi.org/10.1029/2019GL08487

Previdi, M., and L. Polvani, 2014: Climate system response to stratospheric ozone depletion and recovery. *Quarterly Journal of the Royal Meteorological Society*, **140**, 2401–2419. https://doi.org/10.1002/qj.2330

Purich, A., and S.-W. Son, 2012: Impact of Antarctic ozone depletion and recovery on Southern Hemisphere precipitation, evaporation and extreme changes. *Journal of Climate*, **25**, 3145–3154. https://doi.org/10.1175/JCLI-D-11-00383.1

Rae, C., and J. Keeble, P. Hitchcock, and J. Pyle, 2019: Prescribing zonally asymmetric ozone climatologies in climate models: performance compared to a chemistry-climate model. *Journal of Advances in Modeling Earth Systems*, **11**, 918–933. https://doi.org/10.1029/2018MS001478

Randel, W., and E. Jensen, 2013: Physical processes in the tropical tropopause layer and their roles in a changing climate. *Nature Geoscience*, **6**, 169–176. https://doi.org/10.1038/NGEO1733

Randel, W., and F. Wu, 2007: A stratospheric ozone profile data set for 1979–2005: variability, trends, and comparisons with column ozone data. *Journal of Geophysical Research: Atmospheres*, **112**, D06313. https://doi.org/10.1029/2006JD007339

Randel, W., F. Wu, A. Ming, and P. Hitchcock, 2021: A simple model of ozone-temperature coupling in the tropical lower stratosphere, *Atmospheric Chemistry and Physics*, **21**, 18531-186542. https://doi.org/10.5194/acp-21-18531-2021

Raphaldini, B., A. Teruya, P. Leite da Silva Dias, L. Massaroppe, D. Takahashi, 2021: Stratospheric ozone and quasi-biennial oscillation (QBO) interaction

with the tropical troposphere on intraseasonal and interannual timescales: a normal-mode perspective. *Earth System Dynamics*, **12**(1), 83–101. https://doi.org/10.5194/esd-12-83-2021

Reichler, T. and J. Kim, 2008: How well do coupled models simulate today's climate? *Bulletin of the American Meteorological Society*, **89**, 303–311. https://doi.org/10.1175/BAMS-89-3-303

Reynolds, R., T. Smith, C. Liu, D. Chelton, K. Casey, and M. Schlax, 2007: Daily high-resolution-blended analyses for sea surface temperature. *Journal of Climate*, **20**, 5473–5496. https://doi.org/10.1175/ 2007JCLI1824.1

Saggioro, E., and T. Shepherd, 2019: Quantifying the timescale and strength of Southern Hemisphere interseasonal stratosphere-troposphere coupling. *Geophysical Research Letters*, **46**, 13479-13487. https://doi.org/10.1029/2019GL084763

Sakaeda, N., J. Dias, and G. Kiladis, 2020: The unique characteristics and potential mechanisms of the MJO-QBO relationship. *Journal of Geophysical Research: Atmosphere*, **125**, e2020JD033196. https://doi.org/10.1029/2020JD033196

Salby, M., E. Titova, and L. Deschamps, 2011: Rebound of Antarctic ozone, *Geophysical Research Letters*, **38**, L09702. https://doi.org/10.1029/2011GL047266

Seviour, W., S. Hardiman, L. Gray, N. Butchart, C. MacLachlan, and A. Scaife, 2014: Skillful seasonal prediction of the Southern Annular Mode and Antarctic ozone. *Journal of Climate*, **27**(19), 7462–7474. https://doi.org/10.1175/jcli-d-14-00264.1

Shaw, T., J. Perlwitz, N. Harnik, P. Newman, S. Pawson, 2011: The impact of stratospheric ozone changes on downward wave coupling in the Southern Hemisphere. *Journal of Climate*, **24**, 4210–4229. https://doi.org/10.1175/2010JCLI3804.1

Shindell, D., G. Faluvegi, N. Unger, E. Aguilar, G. Schmidt, D. Koch, S. Bauer, and R. Miller, 2006: Simulations of preindustrial, present-day, and 2100 conditions in the NASA GISS composition and climate model G-PUCCINI. *Atmospheric Chemistry and Physics*, **6**, 4427–4459. https://doi.org/10.5194/acp-6-4427-2006

Siegert, S., O. Bellprat, M. Menegoz, D. Stephenson and F. Doblas-Reyes, 2017: Detecting Improvements in Forecast Correlation Skill: Statistical Testing and Power Analysis. *Monthly Weather Review*, **145**, 437-450. https://doi.org/10.1175/MWR-D-16-0037.1

Smith, D., R. Eade, and H. Pohlmann, 2013: A comparison of full-field and anomaly initialization for seasonal to decadal climate prediction. *Climate Dynamics*, **41**, 3325–3338. https://doi.org/10.1007/s00382-013-1683-2

Solomon, S., 1999: Stratospheric ozone depletion: A review of concepts and history, *Reviews of Geophysics*, **37**, 275-316. https://doi.org/10.1029/1999RG900008

Solomon, S., K. Rosenlof, R. Portmann, J. Daniel, S. Davis, T. Sanford, and G.-K. Plattner, 2010: Contributions of stratospheric water vapor to decadal changes in the rate of global warming. *Science*, **327**, 1219–1223. https://doi.org/10.1126/science.1182488

Son, S.-W., N. Tandon, L. Polvani, and D. Waugh, 2009: Ozone hole and Southern Hemisphere climate change. *Geophysical Research Letters*, **36**, L15705. https://doi.org/10.1029/2009GL038671

Son, S.-W., A. Purich, H. Hendon, B.-M. Kim, and L. Polvani, 2013: Improved seasonal forecast using ozone hole variability? *Geophysical Research Letters*, **40**, 6231–6235. https://doi.org/10.1002/2013GL057731

Son, S.-W., Y. Lim, C. Yoo, H. Hendon, and J. Kim, 2017: Stratospheric control of the Madden–Julian Oscillation. *Journal of Climate*, **30**(6), 1909–1922. https://doi.org/10.1175/JCLI-D-16-0620.1

Son, S.-W., B.-R. Han, C. Garfinkel, S.-Y. Kim, R. Park, N. Abraham, H. Akiyoshi, A. Archibald, N. Butchart, M. Chipperfield, M. Dameris, M. Deushi, S. Dhomse, S. Hardiman, P. Jöckel, D. Kinnison, M. Michou, O. Morgenstern, F. O'Connor, L. Oman, D. Plummer, A. Pozzer, L. Revell, E. Rozanov, A. Stenke, K. Stone, S. Tilmes, Y. Yamashita, and G. Zeng, 2018: Tropospheric jet response to Antarctic ozone depletion: An update with Chemistry Climate Model Initiative (CCMI) models, *Environmental Research Letters*, **13**, 054024. https://doi.org/10.1088/1748-9326/aabf21

Son, S.-W., H. Kim, K. Song, S.-W. Kim, P. Martineau, Y.-K. Hyun, and Y. Kim, 2020: Extratropical Prediction Skill of the Subseasonal-to-Seasonal (S2S) Prediction Models. *Journal of Geophysical Research: Atmospheres*, **125**, e2019JD031273. https://doi.org/10.1029/2019JD031273

Steiger, J., 1980: Tests for comparing elements of a correlation matrix, *Psychological Bulletin*, **87**(2), 245-251. https://doi.org/10.1037/0033-2909.87.2.245

Sun, L., H. Wang, and F. Liu, 2019: Combined effect of the QBO and ENSO on the MJO. *Atmospheric and Oceanic Science Letters,* **12**, 170–176. https://doi.org/10.1080/16742834.2019.1588064

Thompson, D., M. Baldwin, and J. Wallace, 2002: Stratospheric connection to Northern Hemisphere wintertime weather: Implications for prediction, *Journal of Climate*, **15**, 1421–1428. https://doi.org/10.1175/1520-0442, 015,1421:SCTNHW.2.0.CO;2

Thompson, A., J. Witte, S. Oltmans, F. Schmidlin, J. Logan, M. Fujiwara, V. Kirchhoff, F. Posny, G. Coetzee, B. Hoegger, S. Kawakami, T. Ogawa, J. Fortuin, and H. Kelder, 2003: Southern Hemisphere Additional Ozonesondes (SHADOZ) 1998–2000 tropical ozone climatology 2. Tropospheric variability and the zonal wave-one. *Journal of Geophysical Research*, **108**(D2), 8241. https://doi.org/10.1029/2002JD002241

Thompson, D., S. Solomon, P. Kushner, M. England, K. Grise, and D. Karoly, 2011: Signatures of the Antarctic ozone hole in Southern Hemisphere surface climate change, *Nature Geoscience*, **4**, 741–749. https://doi.org/10.1038/ngeo1296

Thuburn, J., and G. Craig, 2002: On the temperature structure of the tropical substratosphere. *Journal of Geophysical Research*, **107**(D2), 4017. https://doi.org/10.1029/2001JD000448

Tummon, F., B. Hassler, N. Harris, J. Staehelin, W. Steinbrecht, J. Anderson, G. Bodeker, A. Bourassa, S. Davis, D. Degenstein, S. Frith, L. Froidevaux, E. Kyrölä, M. Laine, C. Long, A. Penckwitt, C. Sioris, K. Rosenlof, C. Roth, H. Wang, and J. Wild, 2015: Intercomparison of vertically resolved merged

satellite ozone data sets: interannual variability and long-term trends. *Atmospheric Chemistry and Physics*, **15**, 3021–3043. https://doi.org/10.5194/acp-15-3021-2015

Tweedy, O., L. Oman, and D. Waugh, 2020: Seasonality of the MJO impact on upper troposphere–lower stratosphere temperature, circulation, and composition. *Journal of Atmospheric Sciences*, **77**(4), 1455-1473. https://doi.org/10.1175/JAS-D-19-0183.1

Vitart, F., C. Ardilouze, A. Bonet, A. Brookshaw, M. Chen, C. Codorean, M. Déqué, L. Ferranti, E. Fucile, M. Fuentes, H. Hendon, J. Hodgson, H.-S. Kang, A. Kumar, H. Lin, G. Liu, X. Liu, P. Malguzzi, I. Mallas, M. Manoussakis, D. Mastrangelo, C. MacLachlan, P. McLean, A. Minami, R. Mladek, T. Nakazawa, S. Najm, Y. Nie, M. Rixen, A. Robertson, P. Ruti, C. Sun, Y. Takaya, M. Tolstykh, F. Venuti, D. Waliser, S. Woolnough, T. Wu, D.-J. Won, H. Xiao, R. Zaripov, and L. Zhang, 2017: The subseasonal to seasonal (S2S) prediction project database. *Bulletin of the American Meteorological Society*, **98**(1), 163–173. https://doi.org/10.1175/BAMS-D-16-0

Waliser, D., K. Sperber, H. Hendon, D. Kim, E. Maloney, M. Wheeler, K. Weickmann, C. Zhang, L. Donner, J. Gottschalck, W. Higgins, I.-S. Kang, D. Legler, M. Moncrieff, S. Schubert, W. Stern, F. Vitart, B. Wang, W. Wang, and S. Woolnough, 2009: MJO simulation diagnostics. *Journal of Climate*, **22**, 3006–3030. https://doi.org/10.1175/2008JCLI2731.1

Wang, S., M. Tippett, A. Sobel, Z. Martin, and F. Vitart, 2019: Impact of the QBO on prediction and predictability of the MJO convection. *Journal of Geophysical Research: Atmospheres*, **124**, 11766–11782. https://doi.org/10.1029/2019JD030575

Waugh, D., C. Garfinkel, and L. Polvani, 2015: Drivers of the recent tropical expansion in the Southern Hemisphere: Changing SSTs or ozone depletion?. *Journal of Climate*, **28**, 6581–6586. https://doi.org/10.1175/JCLI-D-15-0138.1

Walters, D., M. Best, A. Bushell, D. Copsey, J. Edwards, P. Falloon, C. Harris, A. Lock, J. Manners, C. Morcrette, M. Roberts, R. Stratton, S. Webster, J. Wilkinson, M. Willett, I. Boutle, P. Earnshaw, P. Hill, C. MacLachlan, G. Martin, W. Moufouma-Okia, M. Palmer, J. Petch, G. Rooney, A. Scaife, K. Williams, 2011: The Met Office Unified Model Global Atmosphere 3.0/3.1 and JULES Global Land 3.0/3.1 configurations. *Geoscientific Model Development*, **4**, 919–941, https://doi.org/10.5194/gmd-4-919-2011

Wexler, A., 1977: Vapor pressure formulation for ice. *Journal of Research of the National Bureau of Standards—A. Physics and Chemistry*, **81**A, 5–20. https:// doi.org/10.6028/jres.081A.003

Wheeler, M., and H. Hendon, 2004: An all-season real-time multivariate MJO index: development of an index for monitoring and prediction. *Monthly Weather Review*, **132**, 1917–1932. https://doi.org/10.1175/1520-0493(2004)132<1917:AARMMI>2.0.CO;2

Wheeler, M., and K. Weickmann, 2001: Real-time monitoring and prediction of modes of coherent synoptic to intraseasonal tropical variability. *Monthly Weather Review*, **129**, 2677-2694. https://doi.org/10.1175/1520-0493(2001)129<2677:RTMAPO>2.0.CO;2

Wilks, D., 2020: Statistical methods in the atmospheric sciences, 4th edition. Academic, San Diego. https://doi.org/10.1016/C2017-0-03921-6

Xie, F., J. Li, C. Sun, R. Ding, N. Xing, Y. Yang, X. Zhou, and X. Ma, 2018: Improved global surface temperature simulation using stratospheric ozone forcing with more accurate variability. *Scientific Reports*, **8**(1), 14474, https://doi.org/10.1038/s41598-018-32656-z

Xiang, B., M. Zhao, X. Jiang, S. Lin, T. Li, X. Fu, and G. Vecchi, 2015: The 3–4-week MJO prediction skill in a GFDL coupled model. *Journal of Climate*, **28**, 5351–5364. https://doi.org/10.1175/JCLI-D-15-0102.1

Yang, H., L. Sun, and G. Chen, 2015: Separating the mechanisms of transient responses to stratospheric ozone depletion-like cooling in an idealized atmospheric model. *Journal of the Atmospheric Sciences*, **72**(2), 763– 773. https://doi.org/10.1175/JAS-D-13-0353.1

Yoo, C., and S.-W. Son, 2016: Modulation of the boreal wintertime Madden-Julian Oscillation by the stratospheric quasi-biennial oscillation. *Geophysical Research Letters*, **43**,1392–1398. https://doi.org/10.1002/2016GL067762

Yook, S., D. Thompson, S. Solomon, S.-Y. Kim, 2020: The key role of coupled chemistry-climate interactions in tropical stratospheric temperature variability. *Journal of Climate*, **33**, 7619–7629. https://doi.org/10.1175/JCLI-D-20-0071.1

Zhang, C., 2005: Madden Julian Oscillation. *Reviews of Geophysics*, **43**(2), RG2003. https://doi.org/10.1029/2004RG000158

Zhang, C., 2013: Madden–Julian Oscillation: Bridging weather and climate. *Bulletin of the American Meteorological Society*, **94**, 1849–1870. https://doi.org/10.1175/BAMS-D-12-00026.1

# 국문초록

상부대류권과 하부성층권 지역은 적도 지역에서 약 14~20 km, 중·고위도 지역에서는 약 8~20 km 범위에 해당한다. 이 지역은 성층권과 대류권 양 방향의 물질 교환이 이루어지고, 불규칙한 혼합이 발생하여 오존과 같은 화학조성 추정의 불확실성이 크다. 이는 화학 모형이나 기후모형의 오존과 기온 편차 등으로 나타나 모델 예측의 신뢰도뿐만 아니라 전지구 복사 수치에도 큰 영향을 미칠 수 있다. 그러나 대부분의 모델에서는 기후값 오존을 사용하기 때문에 오존의 변동성을 반영하지 못하고 극지역 및 적도 오존 농도를 과대 또는 과소 처방하게 된다. 따라서 모형에서 오존의 중요성을 평가하기 위해 기온 편차와 예측성 측면으로 분리하여 살펴보았다.

첫번째로 영국 기상청 통합모델 기반(AMIP)으로 관측 오존을 이용하여 적도 대류권계면 지역의 기온 편차에 오존의 중요성을 평가하였다. 장기 적분 결과 다른 모델들과 마찬가지로 약 70 hPa 부근의 적도 성층권에서 한랭 편차, 적도 대류권계면에서 약 2 K 가량의 온난 편차 및 성층권 대부분의 지역에서 습윤 편차가 존재하는 것을 확인할 수 있었다. 현업모델에서 사용되는 오존(SPARC)과 관측 오존 자료를 비교한 결과 적도 대류권계면에서 관측에 비해 모델에서

사용하는 오존이 약 40% 가량 많이 존재하였다. 따라서 모델 오존 자료 대신 관측 오존으로 처방한 결과 성층권의 한랭 편차와 적도 대류권계면 부근의 온난 편차가 크게 감소함을 확인하였다. 이는 모델에 비해 관측의 오존량이 감소함에 따라 성층권에 도달하는 장파복사 증가에 의한 것이다. 또한 오존의 배경장 변화에 따라 2차 순환에 의해 극지역의 한랭 편차도 줄어들었다. 오존에 의한 기온 변화는 성층권 습윤 편차도 크게 감소시켰다. 이는 정확한 오존 처방이 모델 수행에 있어서 중요하다는 것을 시사한다.

두 번째로 적도 대류권계면에서 개선된 정적 안정도 변화가 대표적인 성층권과 대류권 커플링 중 하나인 성층권 준 2년주기 진동과 매든-줄리안 진동에 미치는 영향을 살펴보았다. 현업 GloSea5 예측 모형을 이용하여 기후값 오존과 동서 방향의 바람이 동풍 편차인 2006년 사례의 오존을 처방하여 오존-복사 피드백이 대류권에 미치는 영향을 분석한 결과, 해당 연도의 관측 오존을 처방한 경우 관측에 비해 과소 모의되었으나 초기화 후 20일 이후 적도 대류권계면 지역에서 0.4~0.5 K 정도로 약 17%가량 개선되었다. 그러나 두 실험 간의 매든-줄리안 진동의 대류, 진폭과 위상에서는 큰 차이를 볼 수 없었다. 이 연구에서 성층권 준2년주기진동과 매든-줄리안 진동의 상관성을

설명하지 못하는 이유는 성층권 준 2년주기 진동에 대한 하부 성층권 기온 반응의 위치가 제대로 모의되지 않은 것과 관측에 비해 모델에서 매든-줄리안 진동의 대류 자체를 조직화하지 못했기 때문인 것으로 추정된다.

세 번째로 성층권과 대류권 커플링에 있어 남반구 봄철 성층권 오존이 계절 내 규모의 예측성 향상에 미치는 영향을 살펴보았다. 2004년부터 2020년 기후값 오존과 매년 변동하는 오존을 처방하여 매년 9월 1일 초기화 한 결과 두 실험 모두 대류권에서는 몇 주 동안 예측성이 나타나지 않았으나, 약 한달 후 대류권에서 예측성이 다시 나타나는 것을 확인하였다. 성층권과 대류권의 역학적인 커플링에 의해서 발생하는 예측성의 재 출현은 매년 변동하는 오존을 처방한 경우 좀 더 빨리 강하게 나타났다. 또한 대류권뿐만 아니라 지표면의 예측성 또한 향상됨을 확인하였다.

주요어: 성층권-대류권 커플링, 오존-복사 되먹임, 준2년주기 진동, 매든-줄리안 진동, 계절내 계절 예측

학 번: 2009-30863